DISSERTATIONES
SCIENTIAE
MATERIALIS
UNIVERSITATIS
TARTUENSIS
34

ELENA VINOGRADOVA

Optical centers and quantum entangled states of Nd^{3+} ions in doped fluoride crystals

DISSERTATIONES SCIENTIAE MATERIALIS UNIVERSITATIS TARTUENSIS
34

DISSERTATIONES SCIENTIAE MATERIALIS UNIVERSITATIS TARTUENSIS
34

ELENA VINOGRADOVA

Optical centers and quantum entangled states of Nd^{3+} ions in doped fluoride crystals

UNIVERSITY OF TARTU
Press
1632

The study was carried out in the Institute of Physics, Faculty of Science and Technology, University of Tartu.

The Dissertation was admitted on July 3, 2023, in partial fulfilment of the requirements for the degree of Doctor of Philosophy in Material Science and allowed for defence by Scientific Council on Material Science of the Faculty of Science and Technology, University of Tartu.

Supervisors: Dr. hab. Yury Orlovskiy
Institute of Physics, University of Tartu, Estonia

PhD Viktor Peet
Institute of Physics, University of Tartu, Estonia

PhD Ilmo Sildos,
Institute of Physics, University of Tartu, Estonia

Opponent: PhD Sergey Sekatskii
École Polytechnique Fédérale de Lausanne, Switzerland

Defence: August 22, 2023, at University of Tartu, Estonia

This work has been supported by Estonian Research Council grant PRG347. This work has been partially supported by Graduate School of Functional materials and technologies receiving funding from the European Regional Development Fund in University of Tartu, Estonia.

ISSN 2228-0928 (print)
ISBN 978-9916-27-300-5 (print)

ISSN 2806-2574 (pdf)
ISBN 978-9916-27-301-2 (pdf)

Copyright: Elena Vinogradova, 2023

University of Tartu Press
www.tyk.ee

CONTENTS

LIST OF PUBLICATIONS INCLUDED IN THE THESIS

I. Orlovskii, Yu V.; Gross, H.; **Vinogradova, E.E.**; Boltrushko, V.; Hizhnyakov, V. (2020). Spectroscopic evidence of cooperative (entangled) quantum states of Nd^{3+} ion pairs in Nd^{3+}: LaF_3 crystal. Journal of Luminescence, 116920. DOI: 10.1016/j.jlumin.2019.116920.

II. **Vinogradova, E.**; Dolgov, L.; Konyushkin, V.A.; Orlovskaya, E.O.; Vagapova, E.; Treshchalov, A.; Peet, V.; Hizhnyakov, V.; Orlovskii; Yu.V. (2021). Fluorescence of Nd^{3+} optical centers close to cubic symmetry in a calcium fluoride crystal co-doped with Na^{+}. Journal of Luminescence, 234, 117988. DOI: 10.1016/j.jlumin.2021.117988.

III. Orlovskii, Yu.V.; Vagapova, E.A.; Peet, V.; **Vinogradova, E.**; Dolgov, L.; Boltrushko, V.; Hizhnyakov, V. (2022). One- and two-exciton states of pair centers of Kramers Nd^{3+} ions in Nd-doped CaF_2 and SrF_2 crystals, and their possible use as qubits. Journal of Luminescence, 251, 119218. DOI: 10.1016/j.jlumin.2022.119218.

Author's contribution:

I. Fluorescence kinetic measurements, analysis of the fluorescence self-quenching kinetics, participation in data processing, writing a part of the manuscript.

II. Conceptualization, methodology, site-selective laser spectroscopy measurements, fluorescence kinetic measurement, experimental data processing, analysis of the experimental data, comparing calculated and experimental data, writing manuscript draft, review and editing.

III. Site-selective laser spectroscopy measurements, fluorescence kinetic measurements, participation in data processing, writing a part of the manuscript.

Other publications

1. Orlovskii, Y.; **Vinogradova, E.**; Hiznyakov, V. (2019). Cooperative States of Nd^{3+} Ion Pairs and Clusters in Nd^{3+}: LaF_3 crystal. *Conference on Lasers and Electro-Optics Europe & European Quantum Electronics Conference, Munich, Germany, 23–27 June.* IEEE, eb-p-13.
2. **Vinogradova, E**.; Vagapova, E.; Dolgov, L.; Orlovskii, Yu. (2019). Rare earth ions optical centers in inorganic phosphors: from single to entangled states prospective for quantum computing. *Abstract book International research and practice conference Nanotechnology and nanomaterials NANO-2019.* LLC Computer-publishing information center, Kiev, Ukraine, 668−668.

3. Miller, Caius; Puust, Laurits; Ekimov, Evgeny; Vlasov, Igor; Vanetsev, Alexander; **Vinogradova, Elena**; Orlovskii, Yurii; Treshchalov, Aleksei; Sildos, Ilmo (2021). Toward Performance and Applications of Large Area Optical Thermometry Based on the Luminescence of Germanium-Vacancy Defects in Diamond Nanocrystals. Physica status solidi (a), 2000217. DOI: 10.1002/pssa.202000217.
4. Orlovskii Yu., Vagapova E., Peet V., **Vinogradova E**, Dolgov L., Boltrushko V., Hizhnyakov V. (2022). Entangled States in Nd^{3+} Doped Crystals with Fluorite Structure as Qubits. *48th European Conference on Optical Communication, Basel, Switzerland, 18−22 September 2022.* Optica Publishing Group.

I. INTRODUCTION

Fluoride crystals belong to a class of inorganic compounds of alkali earth metal and fluorine. One of their important properties is a wide band gap, which leads to optical transparency in a wide range, including the visible and near-infrared ranges [1, 2]. Doping of fluoride crystals with rare-earth ions (RE ions) ions leads to the formation of different types of optical centers, which are quite stable and highly luminescent. Such optical centers (OC) are of great importance for various application in modern optics and photonics [3–6].

The atomic structure of RE ions is characterized by a Xe core, a partially filled 4f shell, and outer 5*s*-, 5*p*-, 6*s*- shells that shield the 4f shell from the external influences ($[1s^2 2s^2 2p^6 3s^2 3p^6 3d^{10} 4s^2 4p^6 4d^{10}](4f^n)[5s^2 5p^6]$ $(5d^x)(6s^2)$, where x = 1 for La (n = 0), Ce (n=1), Gd (n = 7) and Lu (n = 14); x = 0 for elements from Pr (n = 3) to Yb (n = 14)). This shielding effect protects to some extent the optically active electrons from the influence of the crystal field, leading to the well-defined absorption and emission spectra of RE ions, which are weakly dependent on crystal matrix [7]. The luminescence of RE ions having strong zero-phonon lines (Huang-Rhys factor S << 1) arises due to the electronic transitions inside the $4f^n$ shell rather than the $4f^{n-1}5d^1 \rightarrow 4f^n$ transitions. These transitions in contrast to the latter ones are parity forbidden, but they become partially allowed due to admixing of the 5d orbital wave functions with opposite parity to a 4f wave functions. The value of admixing depends on the crystal matrix and local symmetry of the optical center of a RE ion [7–9].

A RE ion introduced into a crystalline host replaces the host cation and thus forms an optically active center, which exhibits luminescence when excited by an appropriate excitation source [7]. When the replacing ion and the replaced cation are of the same charge, the lattice symmetry at the site may stay the same, and the electroneutrality of the crystal in general is not disturbed [1, 10]. However, if these charges are different, the electroneutrality must be preserved by positioning of a charge compensating lattice ion nearby. This results in a complex set of optical centers in different crystal hosts [11].

In this work, three types of fluoride crystals, LaF_3, CaF_2, SrF_2, doped with Nd^{3+} were studied. The Nd^{3+} is triple-charged, thus there is no need for a compensating ion in the case of LaF_3, where the symmetry of crystal lattice (rhombohedral structure, space group P-3c1) stays undisturbed [10]. However, in the case of the CaF_2 and SrF_2 crystals with fluorite-type structure (both being characterized by cubic structure with space group Fm-3m) a charge compensating ion is needed. This leads to the possibility of formation of different types of optical centers in both the CaF_2 and SrF_2 crystals [11–15].

There are several notable types of Nd^{3+} ion optical centers that can be formed in CaF_2 and SrF_2. The single Nd^{3+} sites with cubic symmetry can be formed in the Nd^{3+}: CaF_2 crystal at low Nd^{3+} concentrations, when their clustering into ion pairs, triplets, quartets, *etc.* does not occur. If alkali-metal ions such as Na^+ are added, and occupy interstitial charge compensators at a considerable

distance, which allows to maintain the cubic symmetry of the lattice, then formation of a single Nd^{3+} sites with cubic symmetry is possible [16, 17]. The pair of substitutional Nd^{3+} and Na^{+} ions has the same positive charge 4+ as the pair of Ca^{2+} ions. Consequently, such charge compensation does not require the presence of interstitial F^{-} ions. Thus, the Nd^{3+} sites with high nearly cubic symmetry close to O_h and non-local charge compensation [16], can be formed.

If additional Na^{+} ion replaces one of the close neighbor Ca^{2+} ions, the formation of single Nd^{3+} sites with C_{2v} symmetry [16], is also possible.

Another type is single-site optical center with tetragonal symmetry C_{4v}, which is lower than the cubic O_h. In this case, the charge compensating ion F^{-} occupies the nearest interstitial position. Such an optical center is usually denoted as the L-center [18, 19]. In addition to single-site centers, pair optical centers consisting of two closely spaced Nd^{3+} ions can be formed. This center has orthorhombic symmetry and denoted usually as M-center [18, 19]. It is also possible to form cluster optical centers with different numbers of ions, for example, triple and quartet centers [11, 12, 18, 19]

While single-site optical centers with C_{4v} symmetry and pair centers of Nd^{3+} ion have been well studied [12, 14, 15, 18, 19, 21–25] the cubic sites in the Nd^{3+}: CaF_2 single crystal were only detected using electron paramagnetic resonance [20, 26]. The high symmetry of the cubic center does not make it possible to remove at least partially the prohibition on the electric dipole transition, which leads to a very weak fluorescence intensity. There were only some short and incomplete reports [16, 23] about long-lived luminescence in Nd^{3+}: CaF_2 that can be hypothetically associated with the cubic sites.

In this work, the new results for the optical centers in Nd^{3+}: CaF_2 and Na^{+}: Nd^{3+}: CaF_2 crystals were obtained. First, an optical center without inversion symmetry in the Nd^{3+}: CaF_2 crystal co-doped with Na^{+}, characterised by C_{2v} symmetry with the long radiative lifetime of τ_R = 8.5 ms was detected and described using the Judd-Ofelt approach. Another center with symmetry close to O_h possessing long radiative lifetime of τ_R = 13.6 ms was also found and described [27].

Recently, an interesting new application field of the pair optical centers of Nd^{3+} ion in fluoride matrices for quantum computing was suggested [28]. Previously, the use of hyperfine levels as qubits in rare earth doped dielectric crystals and nanocrystals (see [29–43] and references therein) was considered. Single qubit gate operations with such qubits require two optical pulses with a very small spectral width of the order of kHz or less. Therefore, such qubits operate with millisecond or longer sampling time. However, as it was shown in [28], the RE ions can also be used for qubits with optical frequencies. In this case, much shorter light pulses can be used allowing much faster QC with nanosecond clock cycles.

It was shown [22, 25, 44–46] that the pair M and the quartet N optical centers of Nd^{3+} ions in the Nd^{3+}: CaF_2 crystal with the heterovalent substitution of Nd^{3+} for Ca^{2+} exhibit strong resonance exchange interaction of electronic excitation between two Nd^{3+} ions. This can happen at liquid helium temperatures or

even higher when the OC is excited at the wavelength resonant with the $^4I_{9/2}(1) \rightarrow {}^4G_{5/2}(1)$ transition between the lowest crystal-field (CF) energy levels of ground and excited manifolds. As a result, the one-exciton $^4I_{9/2}(1)$ x $^4G_{5/2}(1)$ cooperative state of two Nd^{3+} ions becomes entangled. Such centers of RE ions can be very prospective candidates as the elements of quantum logics for quantum computing such as CNOT [28].

The strong resonance exchange of electronic excitation between Nd^{3+} ions is possible in the one-exciton state of the M-center, but such an interaction is absent in the two-exciton excited state $^4G_{5/2}(1)$ x $^4G_{5/2}(1)$ [47]. Thus in [47], the result of the earlier laser pump-probe absorption experiments [48] was confirmed that the exchange of electronic excitation between two Nd^{3+} ions is indeed the main mechanism for the splitting of one-exciton state.

When considering the exchange of electronic excitation between two Nd^{3+} ions, the presence of a half-integer spin and a strong spin-orbit interaction in RE ions should be considered [47] since the electron excitation with spin conservation cannot be the reason for the observed splitting of the one-exciton state of the M center. The spin-orbit interaction does allow the exchange of electronic excitation with a spin flip between Nd^{3+} ions in the M center and the corresponding theory explains well the observed splitting of the one-exciton state [47].

In [28, 47] it was shown that the optical centers of RE ions can be used to perform fast optical QC due to the presence of bright and dark states in these centers: the dark states can be used for qubits, and the bright states are suitable for implementing conditional gate operations.

II. RESEARCH TASK

The goal of the thesis was to study the properties of optical centers in various fluoride crystals such as LaF_3, CaF_2, SrF_2 doped with Nd^{3+} using laser site-selective and kinetic spectroscopy, and to study the formation and the properties of quantum entangled cooperative states of the Nd^{3+} ion pairs.

III. EXPERIMENTAL SET-UP AND SAMPLES

1. Experimental set-up and techniques

Excitation of crystal samples was performed by tunable pulsed Rhodamine 6G dye laser DL-Compact (Estla Ltd., Tartu, Estonia) with the laser line width $\Delta\lambda$ = 0.0065 nm full-width-half-maximum (FWHM), pumped by the second harmonics of Nd:YAG (model LQ215, pulse duration 14 ns, Solar laser systems, Minsk, Belarus). The wavelength of excitation was controlled by the wavelength meter WS 5 (HighFinesse, Graefelfing/Munich, Germany/Ångstrom Ltd., Novosibirsk, Russia) with an accuracy of 0.001 nm.

For the two-color excitation in the spectral range of 564–590 nm, a Continuum Sunlite OPO system PL 9010, TRP with EX OPO frequency extension module (signal 405–705, idler 715–1750 nm, laser line width $\Delta\lambda$ = 0.003 nm at FWHM**)** was used together with the dye laser.

The OPO was pumped by the second harmonics of Continuum Nd:YAG laser with seeder (f = 20 Hz, pulse duration 5 ns).

The whole system and the timing of the laser pulses were synchronized with Digital delay/pulse generator DG645/1 (Stanford Research Systems, Sunnyvale, CA, USA) with the accuracy of 1.5 ns determined by the jitter of the internal pulse generators of Nd:YAG lasers. The laser beams were combined in one path, passed sequentially through two iris diaphragms, and were focused by a lens (f = 180 mm) onto a sample.

The near infrared fluorescence of the sample was focused by a condenser lens on the entrance slit of the Andor Shamrock 750 spectrometer system (Andor, Oxford Instruments, Abingdon-on-Thames, UK) with gratings 300 gr/mm (spectral resolution 0.17nm; linear inverse dispersioon 4.27 nm/mm), 1800 gr/mm (0.03 nm; 0.66 nm/mm), or 2400 gr/mm (0.02 nm; 0.49 nm/mm). The fluorescence was detected with the gated Andor Technology iCCD camera iStar DH320T-18H-13 with the pixel size of 26 μm and with a Peltier cooling system. The FF01-593/LP-25 edge-filter (Shamrock) was placed at the front slit of the monochromator to block the stray light caused by the laser radiation in the case of luminescence detection at the $^4G_{5/2}(1) \rightarrow {}^4I_{11/2}$ and $^4F_{3/2}(1) \rightarrow {}^4I_{9/2}$ transitions.

The upconversion luminescence excitation spectra with two-color excitation pumping were recorded at the $^4D_{3/2}(1) \rightarrow {}^4I_{11/2}(1)$ transition using OPO scanning at the $^4I_{9/2}(1) \rightarrow {}^4G_{5/2}(1)$ transition of the Nd^{3+} ion with simultaneous excitation by a second tunable pulsed dye laser with a fixed wavelength. The fixed laser was in resonance with one of four sublevels of the $^4G_{5/2}(1)$ x $^4I_{9/2}(1)$ one-exciton state.

For fluorescence kinetics measurements, single photon counting Hamamatsu 6240-02 PMT with a PC built-in card multichannel scaler (MSC) was used.

The samples were placed either in the closed-cycle Janis CSS-300S/204N cryostat (USA) and kept at a temperature of 6.5 K, or into a bath cryostat Cryopt A240 (Cryogenic technology laboratory, Institute of Physics NAS of Ukraine) and kept at a selected temperature of 1.6 K, 4.2 K or 7 K.

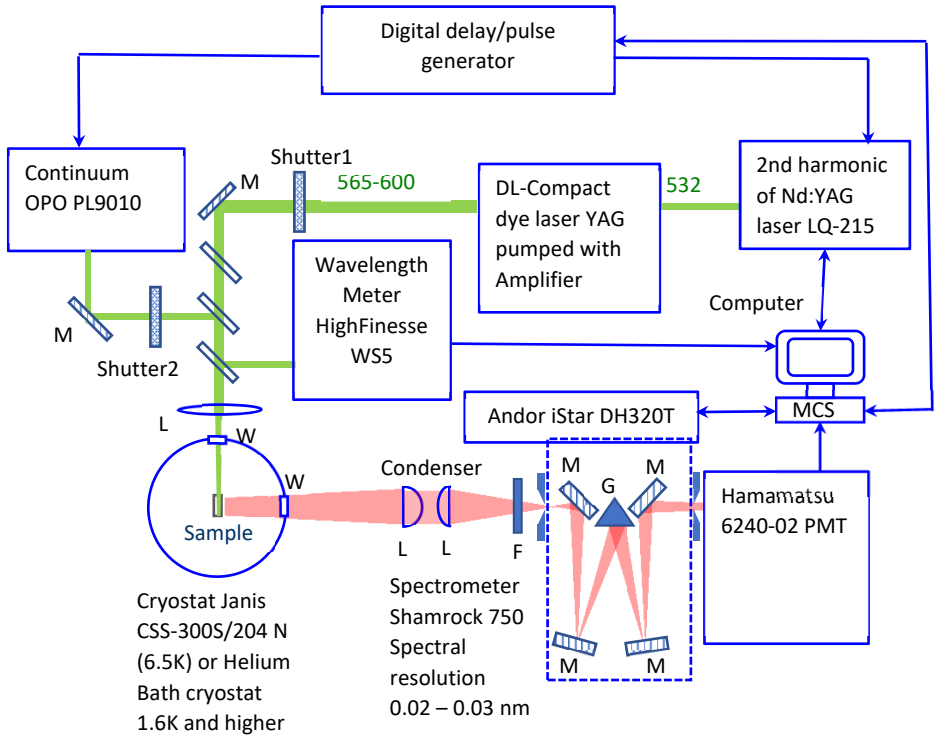

Fig. 1. Schematic of experimental setup

2. Crystals preparation

The oxygen-free Nd^{3+}(0.6%): CaF_2 (type 1) and Nd^{3+}(0.5%): SrF_2 crystals were grown by the Bridgman-Stockbarger technique in fluorine atmosphere at the Division of P.N. Lebedev Physical Institute (USSR) in the 60s of the twentieth century.

The oxygen-free Nd^{3+}(0.03%): CaF_2 (type 1), Nd^{3+}(0.05%): Na^{+}(0.2%): CaF_2 and 1.0 at.% Nd^{3+}: LaF_3 crystals were grown by the Bridgman-Stockbarger technique in fluorine atmosphere at the Prokhorov General Physics Institute (Russia).

IV. EXPERIMENTAL RESULTS AND DISCUSSION

1. Optical centers in the Nd^{3+}: Na^{+}: CaF_2 and the Nd^{3+}: CaF_2 crystals and their type determination

The optical sites with nearly cubic symmetry close to O_h in the Nd^{3+}: Na^{+}: CaF_2 crystal

The existence of the nearly cubic sites with symmetry close to O_h in CaF_2: Nd^{3+} (Fig. 2a) was predicted by crystal-field theory calculations [16], which were confirmed in [27]. The corresponding spectra and kinetics are depicted in Fig.2 of Ref. [27].

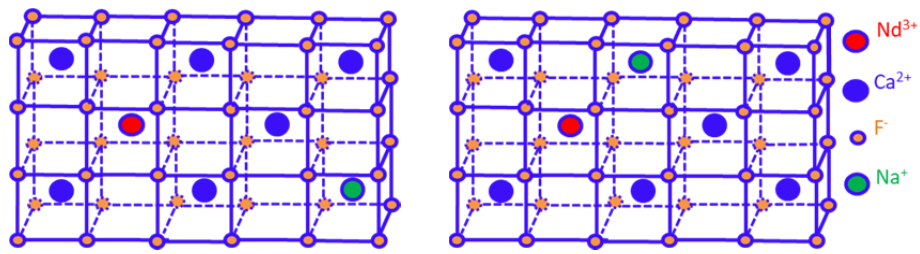

(a) (b)

Fig. 2. Schematic diagram of the Nd^{3+} ion in the nearly cubic site with symmetry close to O_h (a), and in the C_{2v} site (b) in the Nd^{3+}: Na^{+}: CaF_2 single crystal.

The presence of several spectral lines of fluorescence around 860 nm (Fig. 3b, blue) with long lifetimes of the $^4F_{3/2}(1)$ CF level indicates the inhomogeneous splitting of the Nd^{3+} optical centers with the symmetry close to O_h. Moreover, excitation at longer wavelength 584.250 nm (Fig. 3a) reduces strong fluorescence spectral lines around 860 nm and leaves only the second peak at 859.42 nm (Fig. 3b, red). The measured radiative lifetime of the $^4F_{3/2}(1)$ CF level (τ_R = 13.4 ms) associated with these excitation and detection wavelengths (Fig. 6c, red) is slightly less than for optical centers associated with 584.101 nm excitation and 860.70 nm detection wavelengths (τ_R =13.6 ms) (Fig. 3c, green). It should be noted that for the Nd^{3+} ions in crystals, no such long lifetimes have been reported as yet. In the literature, only the results of measuring the fluorescence kinetics in the Nd^{3+}: $Cs_2NaNdC1_6$ elpasolite at 77 K were found so far. The measured lifetime was determined as 11 ms [16].

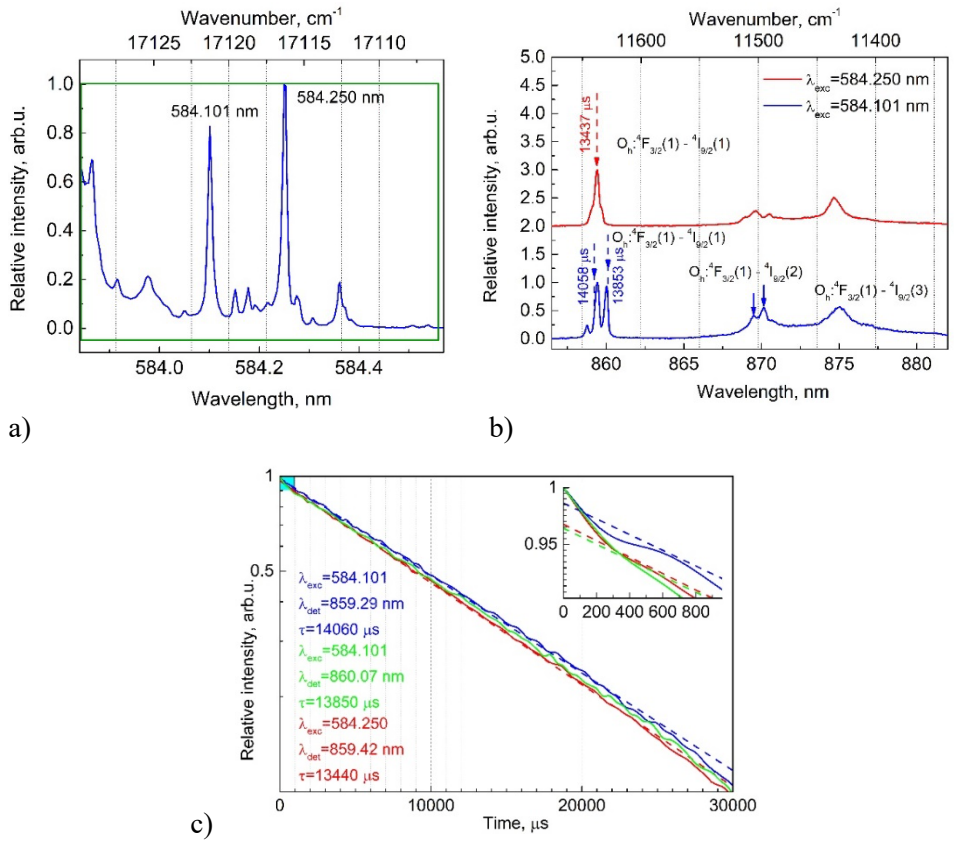

Fig. 3. (a) Fluorescence excitation spectrum in the range of 583.8-584.5 nm wavelengths; (b) fluorescence spectra of the Nd^{3+}(0.05%): Na^{+}(0.2%): CaF_2 single crystal detected at the $^4F_{3/2}(1) \rightarrow {}^4I_{9/2}(1,2)$ transitions at different excitation wavelengths. The longest lifetimes are marked near the corresponding spectral lines; (c) normalized fluorescence kinetics measured for the Nd^{3+}(0.05%): Na^{+}(0.2%): CaF_2 single crystal at different excitation and detection wavelengths: λ_{exc} = 584.101 nm and λ_{det} = 859.29 nm – blue; λ_{exc}=584.101 nm and λ_{det} = 860.07 nm – green; λ_{exc} = 584.250 nm and λ_{det} = 859.42 nm – red. The dashed lines are the approximation with an exponential decay function. The initial stage of the decay curves is shown in the enlarged inset.

The optical sites without inversion symmetry in the Nd^{3+}: Na^{+}: CaF_2 crystal

The most intense spectral line at 583.729 nm of the fluorescence excitation spectrum of the Nd^{3+}(0.05%): Na^{+}(0.2%): CaF_2 crystal at T = 7 K (Fig. 4a, green curve) corresponds to the fluorescence spectral lines at 859.78 nm (11630 cm^{-1}) and 862.08 nm (11600 cm^{-1}) (Fig.4b, green curve). They can be identified as the $^4F_{3/2}(1) \rightarrow {}^4I_{9/2}(1)$ and $^4F_{3/2}(1) \rightarrow {}^4I_{9/2}(2)$ transitions of Nd^{3+} ion in the Na^{+} compensated C_{2v} site (Fig. 2b), since the position of the maxima of their fluorescence spectral lines is in good agreement with the calculated energies 11630 cm^{-1} (859.84 nm) and 11599 cm^{-1} (862.14 nm) given in [16].

The fluorescence kinetics of the $^4F_{3/2}(1)$ CF level, measured at 583.729 nm excitation and 859.78 nm detection wavelengths is a single exponential decay function with the decay time τ = 8.5 ms (Fig. 4c, green curve). In view of the absence of an inversion center in this optical center, the forbidden dipole transition is partially allowed since non-centrosymmetric interactions allow mixing in the electronic states of opposite parity [7–9].

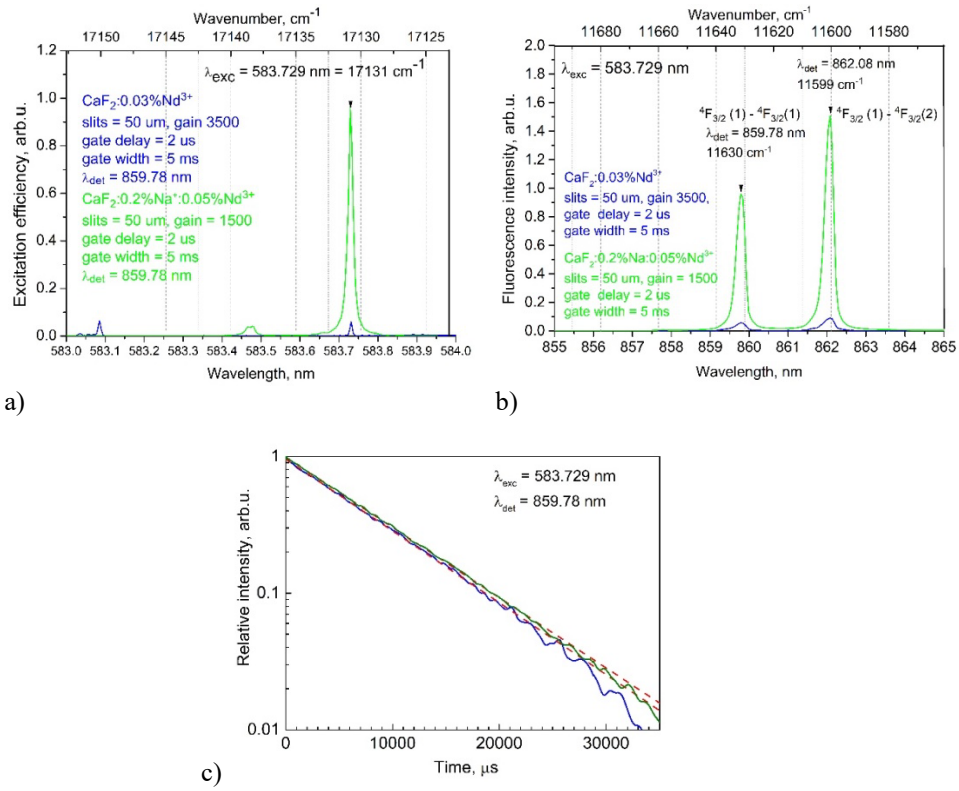

Fig. 4. (a) Fluorescence excitation spectra recorded at the $^4F_{3/2}(1) \rightarrow {}^4I_{9/2}(1,2,3,4)$ transitions of Nd^{3+} in the spectral range of 855–900 nm upon laser tuning at the $^4I_{9/2}(1) \rightarrow {}^4G_{5/2}(1)$ transition, and (b) fluorescence spectra detected at the $^4F_{3/2}(1) \rightarrow {}^4I_{9/2}(1,2)$ transitions at an excitation wavelength of 583.729 nm for Nd^{3+}(0.05%): Na^+(0.2%): CaF_2 – (green curve), and for Nd^{3+}(0.03%): CaF_2 – (blue curve); (c) normalized fluorescence kinetics at λ_{exc}=583.729 nm and λ_{det} = 859.78 nm – Nd^{3+}(0.05%):Na^+(0.2%): CaF_2 (green curve) and Nd^{3+}(0.03%): CaF_2 crystal (blue curve); single exponential decay function with τ_R = 8.5 ms is shown by dashed line.

2. Theoretical discussion of the optical centers' radiative lifetime using Judd-Ofelt approach

Evaluation of the optical centers radiative lifetime using Judd-Ofelt approach

The measured lifetime of the C_{2v} symmetry site of Nd^{3+} $\tau_R = 8.5$ ms is six times that of the C_{4v} site where $\tau_R = 1.4$ ms. Thus, it was observed that the radiative lifetime of the $^4F_{3/2}(1)$ excited state of Nd^{3+} of the higher symmetry site is almost an order of magnitude shorter than for sites with lower symmetry [27].

According to the Judd-Ofelt theory [7–9], the rate of the $|4f\rangle \leftrightarrow |4f'\rangle$ radiative transition is determined by the following equation for the probability of the forced electric dipole transition per unit time

$$A = \frac{4e^2\omega^3}{3\hbar c^3(2J+1)}\left(\frac{n+2}{3n}\right)^2 \sum_{k=2,4,6} \Omega_k \left|U^{(k)}_{ff'}\right|^2. \quad (1)$$

Here e is the electron charge, ω is the frequency of the transition, n is the refractive index of the crystal, c is the speed of light in vacuum, J is the angular momentum of the initial electronic state, Ω_k is the Judd-Ofelt crystal field parameter stemming from the k -th order multipole component of this field, $U^{(k)}_{ff'} = \langle f|\hat{U}^{(k)}|f'\rangle$ is the matrix element of the Judd-Ofelt operator $\hat{U}^{(k)}$, which depends on the radial coordinate r of the optical electron as r^k. In the order of magnitude, the value of the crystal field parameter Ω_k can be estimated from the equation

$$\Omega_k = \alpha_k^2 \Omega_{0k} \left(R_0/R\right)^{4k}, \quad (2)$$

where Ω_{0k} is the Judd-Ofelt crystal field parameter of a Nd^{3+} center of the C_{4v} symmetry, stemming from the k -th order multipole component of the crystal field of a nearest charge compensating F^- ion along the C_4 axis at a distance $R_0 = 0.265$ nm; $R = \sqrt{2}R_0 = 0.375$ nm is the actual distance between the Nd^{3+} and Na^+ ions in the C_{4v} center, α_k is the symmetry factor of the crystal field, which takes into account the dependence of the k -th order electric multipole on the direction of the Na^+ ion compensating the charge; in the order of magnitude $\alpha_k \sim 1$. It is known [49] that for fluoride matrixes doped with Nd^{3+} the radiative decay of the $|^4F_{3/2}\rangle$ state of the Nd^{3+} ion occurs mainly due

to radiative transitions $\left|{}^4F_{3/2}\right\rangle \rightarrow \left|{}^4I_{9/2}\right\rangle$ (contribution 30% to the total decay rate; $U^{(2)}_{ff'}$=0.0000, $U^{(4)}_{ff'}$=0.2293, $U^{(6)}_{ff'}$=0.0548) and $\left|{}^4F_{3/2}\right\rangle \rightarrow \left|{}^4I_{11/2}\right\rangle$ (contribution 50%; $U^{(2)}_{ff'}$=0.0000, $U^{(4)}_{ff'}$=0.1422, $U^{(6)}_{ff'}$=0.4104). Due to the zero values of $U^{(2)}_{ff'}$ for both of these transitions, the contribution of the $\propto \Omega_2$ term to the equation, which takes into account the dipole component of the Stark field of the charge compensating Na^+ ion, disappears, and the nonzero contributions come from the terms $\propto \Omega_4$ and $\propto \Omega_6$. However, due to the large difference $\left(R_0/R\right)^4$ in the depends on the distance R, only the $\propto \Omega_4$ term makes a significant contribution in centers with a charge compensating Na^+ ion located at a distance $R \geq \sqrt{2}R_0$. The contribution of the $\propto \Omega_6$ term is smaller and can be neglected. Therefore, the main contribution to the oscillator strength of the $\left|{}^4F_{3/2}\right\rangle \rightarrow \left|{}^4I_{9/2}\right\rangle$ transitions in C_{2v} and almost cubic symmetry O_h centers on Nd^{3+} in CaF_2 is made by the third-order ($k = 3$, octupole) component of the Stark field of the neighboring Na^+ ion, which compensates for the excess of charge.

The difference in the values of the radiative lifetimes of the C_{4v} and C_{2v} sites can be found from the relations (1), (2) and taking into consideration, that $\tau \sim 1/A$ and $R_{C_{2v}} = \sqrt{2}R_{C_{4v}}$, $\frac{R_{C_{2v}}}{R_{C_{4v}}} = \frac{\sqrt{2}R_{C_{4v}}}{R_{C_{4v}}} = \sqrt{2}$, $\left(\frac{R_{C_{2v}}}{R_{C_{4v}}}\right)^8 = \left(\sqrt{2}\right)^8 = 16$, giving

$$\frac{\tau^{teor.}_{rad}(C_{2v})}{\tau^{teor.}_{rad}(C_{4v})} = \frac{\alpha_4^{C4v}}{\alpha_4^{C2v}}\left(\frac{R_{C_{2v}}}{R_{C_{4v}}}\right)^8 \cong 16\frac{\alpha_4^{C4v}}{\alpha_4^{C2v}} \tag{3}$$

Here $R_{C_{4v}} = R_0 = 0.265$ nm and $R_{C_{2v}} = \sqrt{2}R_{C_{4v}} = 0.375$ nm. According to calculations $\alpha_4^{C4v}/\alpha_4^{C2v} = 0.436$. This gives $\tau^{teor}_{rad}(C_{2v})/\tau^{teor}_{rad}(C_{4v}) = 6.97$, which deviates from the experimental ratio $\tau^{ex.}_{rad}(C_{2v})/\tau^{ex.}_{rad}(C_{4v}) = 8.5\ ms / 1.4\ ms = 6.07$ by 15% only.

Using equations, one can also estimate the difference in the distance of the charge compensating Na^+ ions of C_{2v} center and of almost cubic O_h center as follows

$$\frac{R_{O_h}}{R^{ex}_{C_{2v}}} \approx \sqrt[8]{\frac{\alpha_4^{O_h}}{\alpha_4^{C_{4v}}}\frac{\tau^{ex}_{rad}(C_{O_h})}{\tau^{ex}_{rad}(C_{2v})}} \tag{4}$$

Considering that $\tau_{rad}^{ex}(C_{O_h}) = 13.5\ ms = 1.6\tau_{rad}^{ex}(C_{2v})$ and supposing that $\alpha_4^{O_h}$ and $\alpha_4^{C_{4v}}$ have similar values ($\alpha_4^{O_h} / \alpha_4^{C_{2v}} \approx 1$), $R_{O_h} \approx 1.06 R_{C_{2v}}^{ex} \approx 0.397$ nm.

So, a conclusion can be made that the Judd-Ofelt approach gives not only the rates of radiative relaxation of excited states of a rare-earth ion in different crystal matrices, but also a difference in the rates of emission of an excited state in different optical sites of the same ion in the same crystal matrix. The differences in the distance to a charged compensating ion can lead to inhomogeneous splitting of the spectral lines. The Judd-Ofelt approach can also be used to solve the inverse problem, i.e. to calculate the difference in the distance of the charge compensating ions for different optical centers of the same ion in the same crystal matrix.

3. Optical sites in the Nd^{3+}: LaF_3 crystal

The Nd^{3+} ions in the LaF_3 crystal replace the La^{3+} ions without additional charge compensating ion, thus keeping the local structure of the crystal lattice practically undisturbed (unlike the CaF_2 crystal for example). This allows for a pair of Nd^{3+} ions to have quite high symmetry, which leads to rather small induced dipole momentum. Other optical centers, such as single, triple and quad, also have higher symmetry than in CaF_2 or SrF_2.

The fluorescence excitation spectrum of the 1% Nd^{3+}: LaF_3 crystal at T = 1.6K detected without spectral resolution in the zero-order position of the monochromator grating at the $^4I_{9/2}(1) \rightarrow {}^4G_{5/2}(1)$ transition of the Nd^{3+} ion (Fig. 5) shows a number of well-pronounced spectral lines.

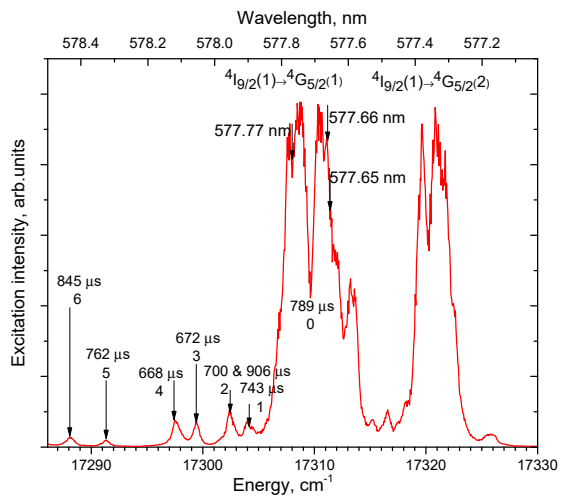

Fig. 5. Time-resolved fluorescence excitation spectrum of the 1 at. % Nd^{3+}: LaF_3 crystal at T = 1.6K detected without spectral resolution in the zero-order position of the monochromator grating at the $^4I_{9/2}(1) \rightarrow {}^4G_{5/2}(1)$ (left strong line) and $^4I_{9/2}(1) \rightarrow {}^4G_{5/2}(2)$ (right strong line) transitions of the Nd^{3+} ion.

After measurement of the fluorescence spectra detected at the $^4F_{3/2}(1) \rightarrow {}^4I_{9/2}(1)$ transition (Fig. 6a), while exciting directly the maxima of each of the spectral lines located at the low energy spectral wing of the measured excitation spectrum (Fig. 5), the corresponding fluorescence kinetics were measured at the fluorescence spectral peaks (Fig. 6b). According to the values of the measured lifetimes it was established that the excitation relaxation is of radiative nature, and the spectral lines correspond to single-site optical centers distorted by nearby defects of crystal lattice. This explains the difference in the spectral line positions and the radiative lifetimes.

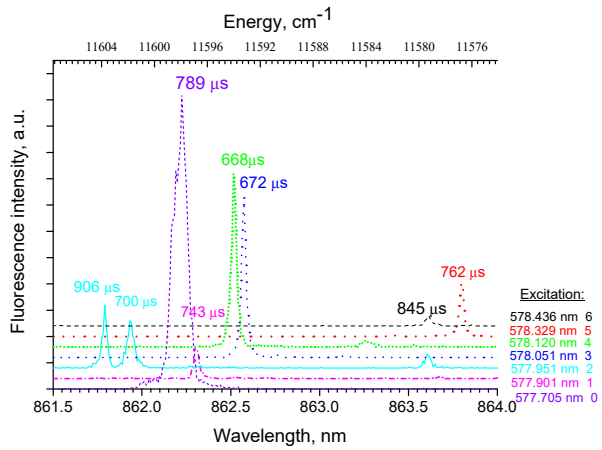

a)

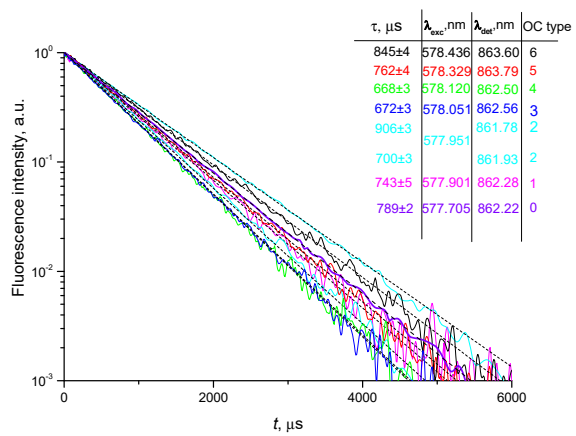

b)

Fig. 6. (a) The luminescence spectra of single-site optical centers at the $^4F_{3/2}(1) \rightarrow {}^4I_{9/2}(1)$ transition of Nd^{3+} in the 1 at.% Nd^{3+}: LaF_3 crystal at T = 4.2 K under selective pulsed laser excitation into maxima of excitation spectral lines marked on the figure. (b) Fluorescence kinetics of the $^4F_{3/2}(1)$ C.F. level of the 1 at.% Nd^{3+}: LaF_3 crystal at T = 4.2 K at different excitation and detection wavelengths.

After measuring of fluorescence spectra, while exciting spectral lines with maxima at 577.65 nm and 577.66 nm (Fig.5), and the corresponding fluorescence kinetics, it was confirmed that these spectral lines correspond to optical centers with different lifetimes determined by radiative and nonradiative excitation relaxation (Fig. 7). To determine the types of these centers, the approach used in [25] for a Nd^{3+}: CaF_2 crystal was used.

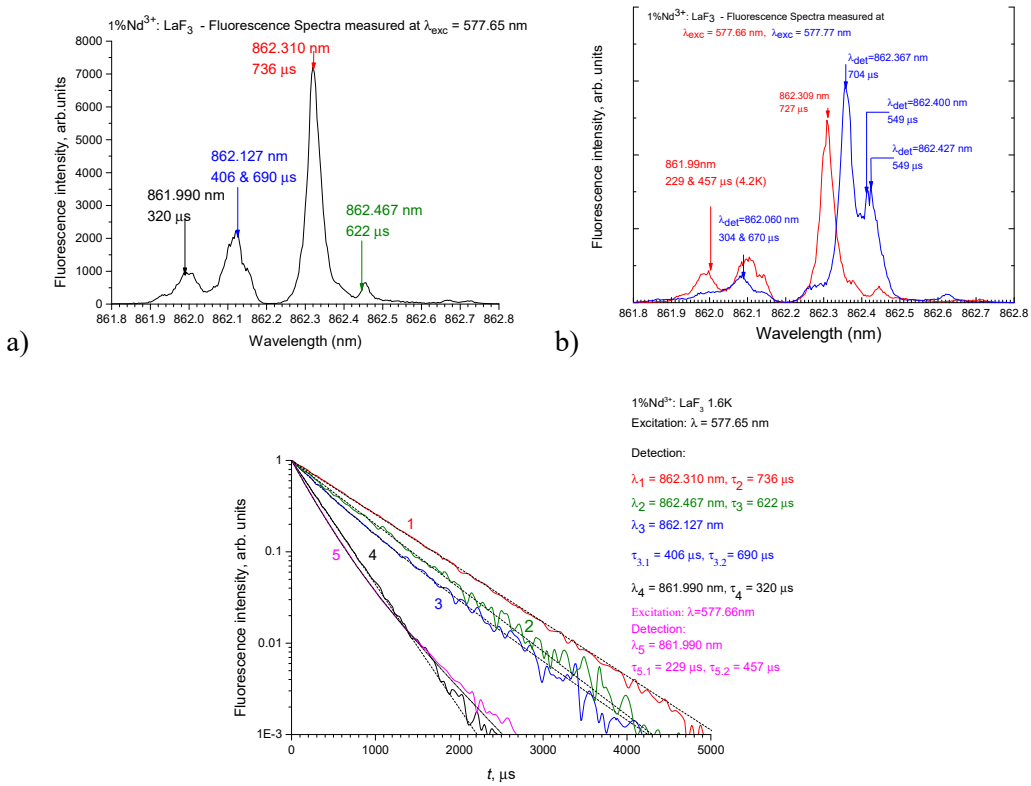

Fig. 7. Fluorescence spectrum at the $^4F_{3/2}(1) \rightarrow {}^4I_{9/2}(1)$ transition of Nd^{3+} of the 1 at.% Nd^{3+}: LaF_3 crystal at T = 1.6K selectively excited at (a) 577.65 nm wavelength, (b) 577.66 nm, and 577.77 nm; (c) the measured fluorescence kinetics of the $^4F_{3/2}(1)$ C.F. level of the 1 at.% Nd^{3+}: LaF_3 crystal at T = 1.6K detected in the maxima of the spectral lines at different excitation and detection wavelengths − solid lines; a curve fit by single or a sum of two exponential curves – dashed lines.

According to this approach, the excited Nd^{3+} ion after fast multiphonon relaxation from the $^4G_{5/2}$ level to the $^4F_{3/2}$ metastable level quenches as a result of incoherent nonradiative resonance energy transfer to an unexcited Nd^{3+} ions in a cluster governed by the $^4F_{3/2} \rightarrow {}^4I_{15/2}$; $^4I_{9/2} \rightarrow {}^4I_{15/2}$ cross-relaxation transitions with the energy transfer rate between two ions calculated as

$$W_{DA} = \frac{1/\tau_{meas} - A}{N-1}, \quad (5)$$

where $A = 1/\tau_R$, $\tau_R = 789$ μs taking for single-site optical center with maximal concentration, and N is the number of ions in the cluster. If we consider the optical center with the decay time $\tau_4 = 320$ μs (Fig. 7c, curve 4) as triple optical center (N - 1 = 2), the calculated value of W_{DA} is 9.29 10^{-4} μs^{-1}. With this value the calculated value of lifetime for the pair center $\tau_{calc}(pair) = \left(W_{DA} + A\right)^{-1}$ = 455 μs, which is very close to experimental one τ_{meas}= 457 μs (Fig. 7c, curve 5). thus this optical center can be considered as a pair center. For quads the calculated $\tau_{calc}(quads) = \left(3W_{DA} + A\right)^{-1}$ = 246 μs is longer than one of the measured lifetimes (τ_{meas} = 229 μs) (Fig. 7c, curve 5), but this can be explained by an increase of spontaneous emission A and energy transfer rates W_{DA} due to increase of line strengths of optical transitions in a quad of Nd^{3+} ions because of stronger crystal field connecting with smaller radius of Nd^{3+} ions comparing to La^{3+} resulting to shorter distance between Nd^{3+} ions. Thus, we consider this optical center as a quad.

Table 1 shows the calculation of the number of Nd^{3+} ions in observed optical centers.

Table 1. Estimation of the number of Nd^{3+} ions in a cluster in the 1 at.% Nd^{3+}: LaF_3 single crystal at T = 1.6K with the measured lifetime of the $^4F_{3/2}(1)$ crystal-field level.

Type of optical center (OC)	Measured lifetime τ, μs	Rate of energy transfer in the pair of Nd^{3+} ions W_{DA}, μs^{-1}	Calculated lifetime τ, μs	N, number of ions in a cluster
Single-site	789	-	-	1
Pair	457	9.29 10^4; τ_{tr} =10.8 μs	455	2
Triple	320	W_{DA}^{meas} = 9.29 10^4	320	3
Quad	229	9.29 10^4	246	4

Another interesting result was experimentally observed after analysis of the fluorescence excitation spectra at the $^4I_{9/2}(1) \rightarrow {}^4G_{5/2}(1)$ transition with fluorescence detection at the $^4F_{3/2}(1) \rightarrow {}^4I_{9/2}(1)$ transition at 861.990 nm. The spectral dip between two spectral peaks with energy difference of 0.2 cm^{-1} demonstrates the entanglement of the $^4I_{9/2}(1)$ x $^4G_{5/2}(1)$ cooperative state of the Nd^{3+} ions in the Nd^{3+}: LaF_3 crystal (Fig.8).

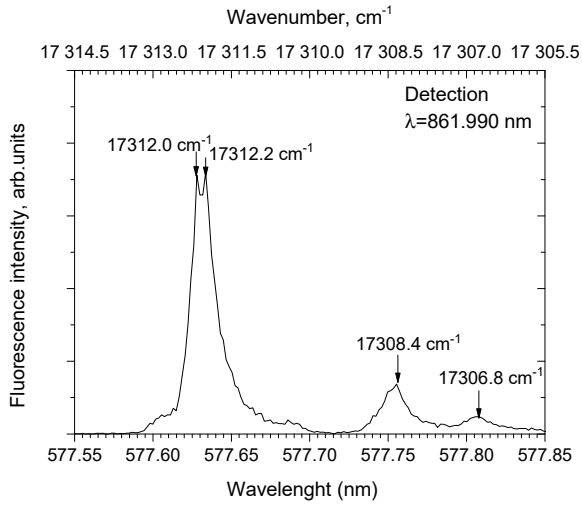

Fig.8 Fluorescence excitation spectrum at the $^4I_{9/2}(1) \rightarrow {}^4G_{5/2}(1)$ transition and detected at the $^4F_{3/2}(1) \rightarrow {}^4I_{9/2}(1)$ transition at 861.990 nm.

To confirm the formation of the entangled $^4I_{9/2}(1)$ x $^4G_{5/2}(1)$ cooperative state of the Nd^{3+} ions in the Nd^{3+}: LaF_3 crystal, the experimental spectrum (Fig.8) was compared to theoretically simulated shape of the spectrum of an entangled cooperative state. [50]

4. Theoretical derivation of the entanglement state function for pair centers in LaF_3: Nd^{3+} crystal

Due to the difference in crystal field for different pair centers, the frequencies of the electronic transition in ions and the resonance interaction Γ in the pair optical centers can be different. The distribution function of the frequency of singlet-singlet electronic transitions in a single-ion optical centers in the case of the inhomogeneous field stemming from dipole-dipole interaction of ions with randomly distributed defects in the crystal lattice is Lorentzian [51].

The resulting spectrum of the optical $^4I_{9/2}(1)$ x $^4I_{9/2}(1) \rightarrow {}^4G_{5/2}(1)$ x $^4I_{9/2}(1)$ transition is described by the following formula

$$J_{\pm}(\omega) = I_{0n} \sum_n \frac{\frac{(1 \mp \frac{\bar{\Gamma}}{\Omega})\bar{\gamma}_n \bar{\varepsilon}_{\pm}}{\pi}}{\left(\sqrt{|(\omega-\omega_n)^2 - \Gamma_0^2|} - \Delta_0\right)^2 + \bar{\varepsilon}_{\pm}^2} \qquad (6)$$

Here it is considered that the value of $\bar{\varepsilon}$ is different for positive and negative ω- ω_n and ω_n is spectral positions of the line number n given by the energy difference of the participating states.

For $T=1.6\mathrm{K}$ the Boltzmann population factor factor $e^{\frac{-\hbar\omega_l}{k_B T}}$ for the singlet level in the ground state is very low and, therefore, transitions from this level are neglected.

The n stands for the number of allowed optical transitions from the one-exciton state presented in Table 2, $\bar{\gamma}_n = \gamma_0'(1 \pm \Gamma/\Omega) e^{\frac{-\hbar\omega_n}{k_B T}}, n \le 8$, and $\bar{\gamma}_n = \gamma_0''(1 \pm \Gamma/\Omega)\, e^{-\hbar\omega_n/k_B T}$, $n \ge 9$. $\gamma_0 = \gamma_0' + \gamma_0''$, is the total rate of transitions from the one-exciton state, where γ_0' is the rate of transitions with the same direction of spin in both ground and excited states (transition without spin-flip, and γ_0'' is the rate of transitions with changed direction of spin (transition with spin-flip). The rates of radiative transitions of the cooperative states can be expressed via the product of γ_0' or γ_0'' and the factors $1+|\Gamma|/\Omega$ corresponds to the bright states, or $1-|\Gamma|/\Omega$ corresponds to the dark states (Table 2). If $\left|\frac{\Delta}{\Gamma}\right| \ll 1$ then the bright states have radiative decay rate almost twice as large as for single-site optical center; the dark states are almost nonradiative.

Table 2. The rates of radiative transitions of the ${}^4G_{5/2}(1)\, x\, {}^4I_{9/2}(1)$ cooperative state of the pair centers of the Nd^{3+} ion.

Transitions	Rates
$T_0^g \leftrightarrow T_{0;+}^e$ $\begin{pmatrix} T_1^g \leftrightarrow T_{1;+}^e \\ T_2^g \leftrightarrow T_{2;+}^e \end{pmatrix}$ $S^g \leftrightarrow S_+^e$	$\gamma_0'(1+\Gamma/\Omega)$
$T_0^g \leftrightarrow T_{0;-}^e$ $\begin{pmatrix} T_1^g \leftrightarrow T_{1;-}^e \\ T_2^g \leftrightarrow T_{2;-}^e \end{pmatrix}$ $S^g \leftrightarrow S_-^e$	$\gamma_0'(1-\Gamma/\Omega)$
$\begin{pmatrix} T_0^g \leftrightarrow T_{1;+}^e \\ T_0^g \leftrightarrow T_{2;+}^e \end{pmatrix}$ $\begin{pmatrix} T_1^g \leftrightarrow T_{0;+}^e \\ T_2^g \leftrightarrow T_{0;+}^e \end{pmatrix}$ $\begin{pmatrix} T_1^g \leftrightarrow S_-^e \\ T_2^g \leftrightarrow S_-^e \end{pmatrix}$ $\begin{pmatrix} S^g \leftrightarrow T_{1;-}^e \\ S^g \leftrightarrow T_{2;-}^e \end{pmatrix}$	$\gamma_0''(1+\Gamma/\Omega)/2$
$\begin{pmatrix} T_0^g \leftrightarrow T_{1;-}^e \\ T_0^g \leftrightarrow T_{2;-}^e \end{pmatrix}$ $\begin{pmatrix} T_1^g \leftrightarrow T_{0;-}^e \\ T_2^g \leftrightarrow T_{0;-}^e \end{pmatrix}$ $\begin{pmatrix} T_1^g \leftrightarrow S_+^e \\ T_2^g \leftrightarrow S_+^e \end{pmatrix}$ $\begin{pmatrix} S^g \leftrightarrow T_{1;+}^e \\ S^g \leftrightarrow T_{2;+}^e \end{pmatrix}$	$\gamma_0''(1-\Gamma/\Omega)/2$
$T_0^g \leftrightarrow S_\pm^e$ $\begin{pmatrix} T_1^g \leftrightarrow T_{2;\pm}^e \\ T_2^g \leftrightarrow T_{1;\pm}^e \end{pmatrix}$ $S^g \leftrightarrow T_{0;\pm}^e$	0

Here Γ is the resonance interaction parameter (Rabi frequency); Ω is the generalized Raby frequency determined as half-frequency difference between singlet (triplet) states; ω_0 is the average frequency of the electronic transition in the pair optical center, Δ is the half-energy difference between states of ions in the pair. As the fluctuations of Δ and Γ are only partly independent, it is considered that $\Delta = \Delta_0 + \xi$ and $\Gamma = \Gamma_0 + \lambda\xi + \sigma$, where Δ_0 and Γ_0 stand for the mean values of Δ and Γ, respectively; ξ, $\lambda\xi$ and σ account for the variations of these quantities due to the interaction of the pair center with random crystal field: ξ accounts for the variations of Δ and for the mutual variations with Γ, and σ accounts for the variations of Γ independent from the variations of Δ (Fig.9).

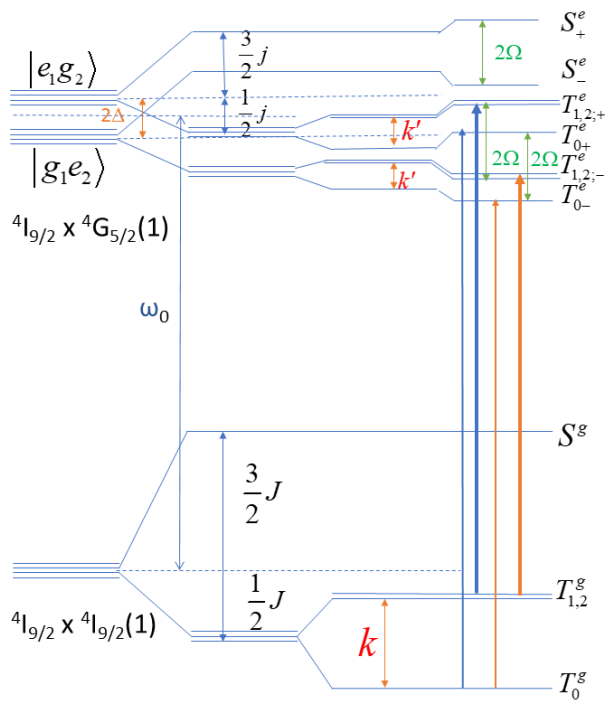

Fig.9. Energy level diagram of the $^4I_{9/2}(1)$ x $^4I_{9/2}(1) \rightarrow {}^4G_{5/2}(1)$ x $^4I_{9/2}(1)$ transition for an exchanged coupled pair of the Nd^{3+} ions; here ω_0 is the average frequency of the electronic transition in the pair optical center, Δ is the half-energy difference between states of different ions in the pair, Γ is the resonance interaction parameter, *k, k'* – shift between T_0 and $T_{1,2}$ states.

The resulting theoretical spectrum fits well with the experimental one (Fig. 10) with the parameters used in [50].

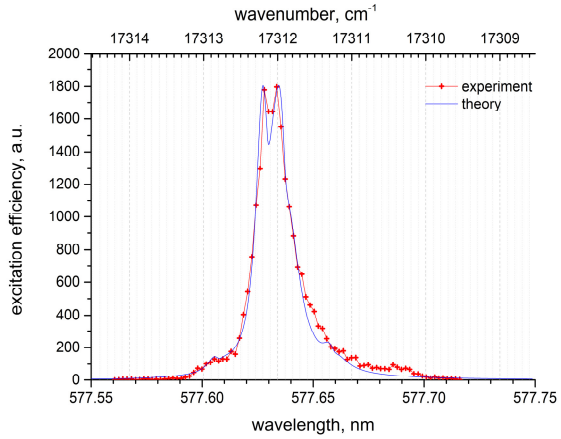

Fig. 10. Fluorescence excitation spectra measured at the $^4I_{9/2}(1) \rightarrow {}^4G_{5/2}(1)$ transition and detecting at 861.990 nm at the $^4F_{3/2}(1) \rightarrow {}^4I_{9/2}(1)$ transition of the 1 at.% Nd^{3+}: LaF_3 crystal at $T = 1.6$K. Red curve with crosses – experiment, blue curve – theory.

The most important feature of the spectrum is the presence of a narrow dip in the line center. This dip is a consequence of the exchange interaction Γ; this interaction not only excludes the crossing of levels in an inhomogeneous crystal field, but also demonstrates the presence of the dark states of pair centers with $|\Delta| \ll |\Gamma|$ at small negative values of $\omega - \omega_0$. The difference between experiment and theory at the low-energy sideband can be attributed to a small contribution of the fluorescence of triple and quad optical centers with lower concentrations and lower fluorescence intensities compared to the pair center.

5. The pair optical sites in the Nd^{3+}: SrF_2 crystal

In this work, the spectral selection of at least two new types of pair optical centers of the Nd^{3+} ion similar to the M-type center in the Nd^{3+}: CaF_2 crystal has been carried out.

The excitation spectrum of the one-exciton state of the M_1 pair center in the Nd^{3+}: SrF_2 crystal at a temperature of 6.5 K shows three pronounced spectral peaks with a splitting of 3.0 cm^{-1} (Fig. 11c, right), while for the M center in the Nd^{3+}: CaF_2 crystal at 6.5 K this splitting is 2.2 cm^{-1} (Fig. 11c, left). The inhomogeneous splitting of the pair centers in the Nd^{3+}: SrF_2 crystal at T = 6.5K (two different types of pair M centers) was detected due to the significant difference in the lifetimes of the two types of pair centers, M_1 and M_2 (Fig. 11d). The lifetime of the M_2 pair center, $\tau = 259$ μs (Fig. 11d, violet curve) is longer than that of M_1 center, $\tau = 167$ μs (Fig. 11d, red curve). The luminescence spectrum of pair M_2 centers (Fig. 11b) has a pronounced spectral peak at the $^4F_{3/2}(1) \rightarrow {}^4I_{9/2}(1)$ transition with a maximum at wavelength of 863.37 nm,

that is, it is shifted by 0.07 nm to the longer wavelengths relative to the pair M_1 center (Fig. 11a). In the fluorescence excitation spectrum of the single-exciton state of M_2 pair centers in the Nd^{3+}: SrF_2 crystal at T = 6.5 K, three spectral peaks are observed with an inhomogeneous broadening of each of them within 1 cm^{-1} (Fig. 11c, violet curve). the total splitting of the M_2 centers is 1.5 times less (2.0 cm^{-1}) compared to the splitting of the M_1 centers (3.0 cm^{-1}). This can be related to the distance of the Nd^{3+} ions in the pair, since the greater this distance, the weaker is the electric quadrupole-quadrupole exchange interaction between them and the smaller the splitting of the one-exciton state.

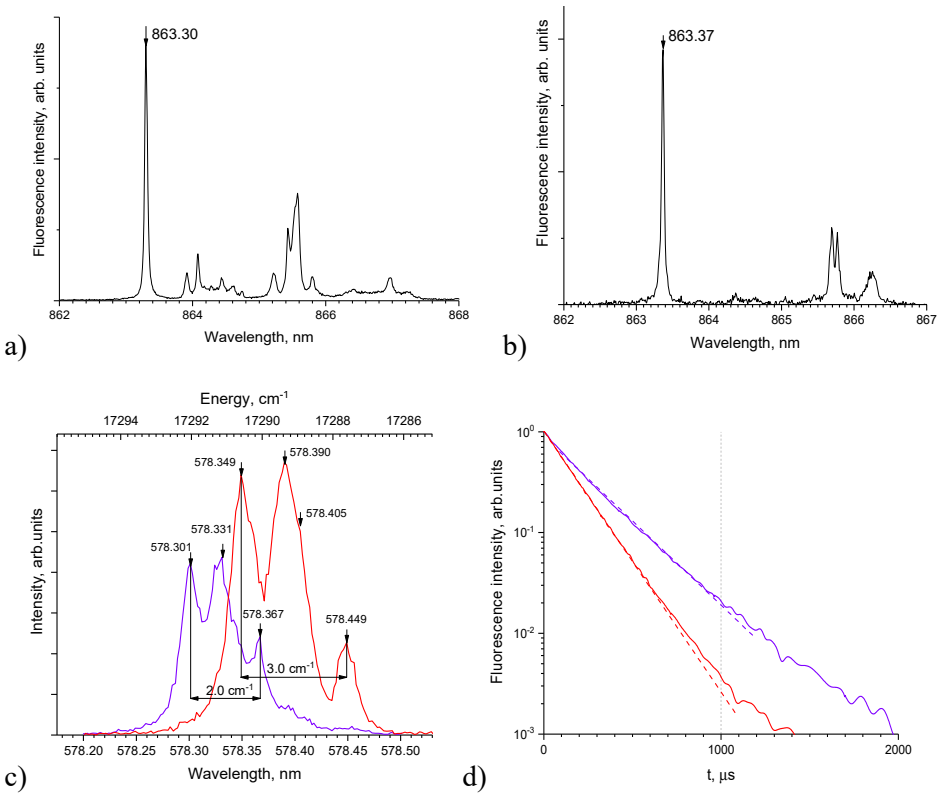

Fig. 11. Fluorescence spectra of two types of pair optical centers in 0.5% Nd^{3+}: SrF_2 at T = 6.5K detected at the $^4F_{3/2}(1) \rightarrow {}^4I_{9/2}$ transition with zero gate delay at different excitation wavelengths: a) 578.398 nm, gate width of 1.1 ms (M_1); b) 578.300 nm, gate width of 0.8 ms (M_2); c) Fluorescence excitation spectra of the one-exciton $^4G_{5/2}(1)$ x $^4I_{9/2}(1)$ states of the 0.5% Nd^{3+}: SrF_2 crystal at T = 6.5K when scanning tunable OPO at the $^4I_{9/2}(1) \rightarrow {}^4G_{5/2}(1)$ transition and detected: at 863.30 nm with the gate delay of 20 ns and gate width of 300 μs (M_1) – red curve; and at 863.36 nm with the gate delay of 650 μs and gate width of 350 μs (M_2) – violet curve; d) Fluorescence kinetics of the 0.5% Nd^{3+}: SrF_2 crystal at T= 6.5K at different excitation and detection wavelengths: excitation at 578.353 nm, detection at 863.30 nm, τ = 167 μs (M_1) – red curve, and excitation at 570.300nm, detection at 863.36 nm, τ = 259 μs (M_2) – violet curve.

For the pair M_1 center in the 0.5% Nd^{3+}: SrF_2 at T = 6.5K crystal, the up-conversion luminescence excitation spectrum was measured (Fig. 12a, black curve) by scanning the dye laser at the $^4G_{5/2}(1) \rightarrow {}^4I_{9/2}(1)$ transition and luminescence detection at the $^4D_{3/2}(1) \rightarrow {}^4I_{11/2}(1)$ transition at 379.77 nm (Fig. 12b). As in the case of the pair M center in the Nd^{3+}: CaF_2 crystal, upon excitation by only one tunable dye laser, only one pronounced spectral peak is observed when two excitation photons of the same frequency are in resonance with the two-exciton cooperative state $^4G_{5/2}(1)$ x $^4G_{5/2}(1)$, and the first photon from the pair is in resonance with the one-exciton cooperative state $^4G_{5/2}(1)$ x $^4I_{9/2}(1)$. The inhomogeneous width of this line, which is at least two orders of magnitude larger than the homogeneous one [44], determines the energy spread in the position of the two-exciton state, which is approximately 1 cm^{-1}. The splitting of two-exciton state in Nd^{3+}: SrF_2 at T = 6.5K caused by the magnetic dipole-dipole interaction is comparable with that in Nd^{3+}: CaF_2, which is ~ 0.2 cm^{-1} [22, 47, 48].

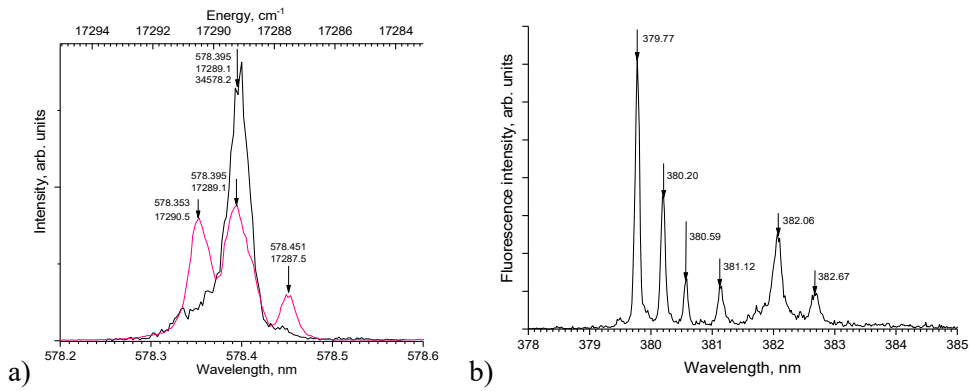

Fig. 12. a) Fluorescence excitation spectra of one- ($^4G_{5/2}(1)$ x $^4I_{9/2}(1)$) and two-exciton ($^4G_{5/2}(1)$ x $^4G_{5/2}(1)$) states of the pair M_1 center in the 0.5% Nd^{3+}: SrF_2 crystal at T = 6.5 K normalized to the area when scanning the tunable dye laser at the $^4G_{5/2}(1) \rightarrow {}^4I_{9/2}(1)$ transition with a step of 0.0025 nm with zero gate delay and fluorescence detection at: 863.30 nm and gate width of 1100 μs − red curve; 379.77 nm and gate width of 400 ns − black curve. b) Upconversion luminescence spectrum of the pair M_1 center of the 0.5% Nd^{3+}: SrF_2 crystal at T = 6.5K excited at 579.397 nm with zero gate delay and the gate width of 500 ns.

A confirmation of the larger distance in the M_2 pair center is the longer lifetime of the $^4F_{3/2}(1)$ state, which is mainly determined by the incoherent electric dipole-dipole interaction in the Nd^{3+} - Nd^{3+} pair, and depends on the distance as $1/R^6$ [25]. Using simple calculations, one can determine the ratio of distances between neodymium ions in pair centers of two types with different distance between ions.The fluorescence quenching rate of the $^4F_{3/2}(1)$ level of the Nd^{3+}

ion of the *i*-th pair center W_i is determined by the sum of the rates of radiative spontaneous decay A_i and the rate of incoherent quenching in the pair C_{DA}/R^6 [25]

$$W_1 = A_1 + C_{DA}/R_1^6 \tag{7}$$

$$W_2 = A_2 + C_{DA}/R_2^6 \tag{8}$$

where C_{DA} is a microparameter of the donor-acceptor interaction, which does not depend on the distance in a pair of neodymium ions.

Assuming that $A_i \ll C_{DA}/R_1^6$ [25] and $C_{DA} = const$ (a necessary condition for the latter should be the equality of the rates of spontaneous emission in the donor and the absorption cross sections in the acceptor for both types of pair centers, i.e. $A_1 = A_2$, and $\sigma_1 = \sigma_2$), the ratio can be determined

$$\frac{W_1}{W_2} = \left(\frac{R_2}{R_1}\right)^6 = \frac{260}{165} = 1.576\ , \tag{9}$$

which gives $R_2/R_1 = 1.08$. Assuming that the splitting due to the strong resonant exchange quadrupole–quadrupole interaction in a pair of neodymium ions in the one-exciton state is proportional to $1/R^5$ [45], the ratio of splitting values in two types of pair M centers with different distances in the pair is $\alpha_1/\alpha_2 = (R_2/R_1)^5 = (1.08)^5 = 1.46$, which agrees very well with the ratio obtained experimentally, $\alpha_1^{exp}/\alpha_2^{exp} = 3/2 = 1.5$.

As in the case of the pair M center in the Nd^{3+}: CaF_2 crystals, the observed splitting of the one-exciton $^4G_{5/2}(1)$ x $^4I_{9/2}(1)$ state for the pair M_1 and M_2 centers in the Nd^{3+}: SrF_2 crystal is of the order of several cm^{-1}. It is determined by strong resonance electric exchange interaction. The spectral linewidth of the two-exciton state $^4G_{5/2}(1)$ x $^4G_{5/2}(1)$ of the pair M_1 center, like the pair M center in the Nd^{3+}: CaF_2 crystal, is determined only by the inhomogeneous broadening due to the absence of the electrical resonance exchange interaction between two excited Nd^{3+} ions [47, 48].

6. Two-exciton states of pair centers of Kramers Nd^{3+} ions in Nd^{3+}-doped CaF_2 crystal

The strong crystal field of cubic symmetry resulting from the eight nearest F^- ions splits the $^4I_{9/2}$ state into three states: two quartets belonging to Γ_8 irreducible representations of the O_h symmetry point group, and one Kramers doublet belonging to Γ_7 irreducible representations of this group. The Stark

splitting is several hundreds of cm^{-1} [14, 16]. The lowest energy state is a quartet of Γ_8 irreducible representation. In the rhombic (C_{2v} symmetry) crystal field of the M center it splits by 31 cm^{-1} into two Kramers doublets belonging to Γ_5 irreducible representations of the point group C_{2v} (see [16], Table 4.26)]. Thus, the ground state of the M-center is a Kramers doublet. The excited $^4G_{5/2}$ state splits in a field of cubic symmetry into one quartet Γ_8 and one Kramers doublet of representation Γ_7 with the energy difference of 181 cm^{-1} [16]**.** The state of representation Γ_7 has lower energy; in the point group C_{2v} it transforms in accordance with Γ_5 irreducible representations and is responsible for the optical transitions observed here with the mean frequency $\omega_0 \cong 17260.2$ cm^{-1}.

The upconversion luminescence excitation spectra of the pair M center in the 0.6% Nd^{3+}: CaF_2 crystal with biharmonic pumping were recorded at the $^4D_{3/2}(1) \rightarrow {}^4I_{11/2}(1)$ transition. In each excitation spectra, distinct narrow peak was observed upon excitation into each energy sublevel of the one-exciton state and the sum of the energies of the resulting spectral peak and the fixed dye laser was $2\omega_0 = 34520.2 \pm 0.2$ cm^{-1} (see, e.g., Fig. 13, dark green).

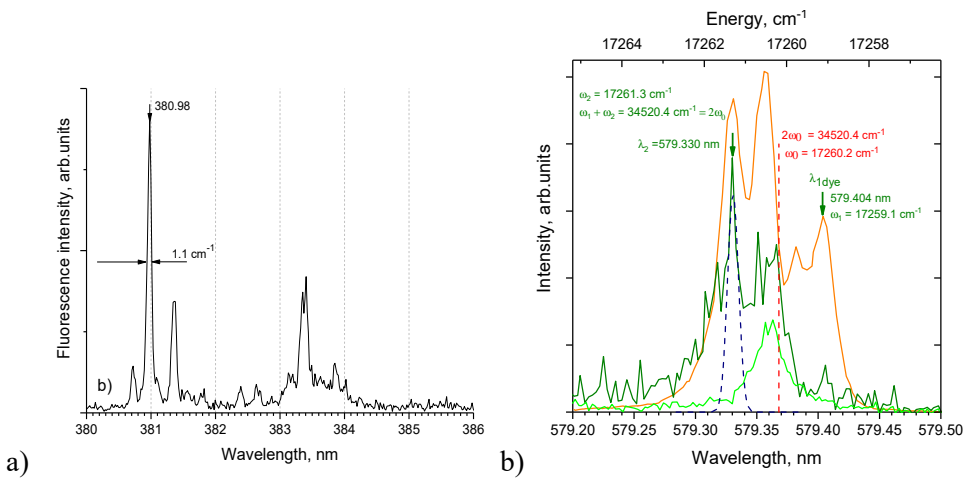

Fig. 13. a) Fluorescence spectra of pair optical M centers in the 0.6% Nd^{3+}: CaF_2 at T = 6.5K at 578.357 nm excitation wavelengths detected with zero gate delay and gate width Δt = 400 ns at the $^4D_{3/2}(1) \rightarrow {}^4I_{11/2}$ (1) transition. b) Fluorescence excitation spectra of the one- $^4G_{5/2}(1)$ x $^4I_{9/2}(1)$ and the two- $^4G_{5/2}(1)$ x $^4G_{5/2}(1)$ exciton states of the 0.6% Nd^{3+}: CaF_2 crystal at T = 6.5K measured by scanning OPO at the $^4I_{9/2}(1) \rightarrow {}^4G_{5/2}(1)$ transition: NIR fluorescence recorded at the $^4F_{3/2}(1) \rightarrow {}^4I_{9/2}(1)$ transition at 863.56 nm – orange curve; upconversion UV fluorescence recorded at the $^4D_{3/2}(1) \rightarrow {}^4I_{11/2}(1)$ transition at 380.98 nm: under excitation by tuned OPO – green curve; under simultaneous excitation by tuned OPO and dye laser fixed at 579.404 nm (shown by arrow) – dark green curve; Gaussian peak positioned at 579.331 nm according to $\omega_{dye} + \omega_{OPO}=2\omega_0$ – blue dashed curve. The position of ω_0 is shown by vertical dashed red line.

The one-color excitation spectrum of NIR fluorescence has four well-pronounced spectral peaks known from previous studies (Fig. 13b, orange curve) [22, 25, 45, 48]. For the laser pulse energy of up to 300 μJ, the intensity of all four peaks was proportional to the pulse energy, which indicated the absence of saturation. The estimated width of spectral peaks is about 0.5 cm^{-1}, which exceeds more than twice the laser line width of 0.2 cm^{-1}. This results from the inhomogeneous broadening and unresolved internal structure of the M-center absorption lines. The homogeneous width of fine-structure components is 0.0017 cm^{-1} [44].

With single-color excitation to the one-exciton state, the M-center can absorb another photon of the same frequency. It leads to the formation of doubly-excited M center (two-exciton state), which can be monitored by the UV upconversion luminescence at the $^4D_{3/2}(1) \rightarrow {}^4I_{11/2}(1)$ transition of Nd^{3+} ions detected at 380.98 nm (Fig. 13a). The excitation spectrum of such an UV luminescence obtained in Nd^{3+}: CaF_2 using only one scanned OPO (Fig. 13b, green curve) is very similar to that obtained in [22] with the same sample.

The one-color excitation band of doubly excited M-centers in Nd^{3+}: CaF_2 has maximum at 17260.5 cm^{-1} in one-photon scale. Contrary to the four-lines spectrum of the parent one-exciton state, the spectral band of doubly-excited M center has no detectable substructure. It agrees with previous experimental observations [22].

The absorption spectra of M centers under two-color laser excitation were examined in [48] using pump-probe technique. Here a similar two-color dye laser and OPO excitation scheme is applied, but controlled the intensity of the UV luminescence, resulting in a much higher sensitivity. Besides, in this case both laser sources had comparable pulse energy. This made it possible to initiate several one- and two-color excitation channels involving various combinations of absorbed photons. The pulses of both light sources overlap in time and their intensity maxima coincide.

One of the examples of two-color excitation spectra obtained when the dye laser was fixed at the position of the spectral peak at 579.404 nm, which corresponds to the lowest of the four energy levels of one-exciton state (Fig. 13b, orange line). The two-color excitation spectrum has one well pronounced sharp spectral peak (Fig. 13b, dark green line). This spectral peak is an analogue of the anti-hole observed in absorption spectra of Ref. [48], where it appeared as a result of the laser-induced excited state absorption. The most intense part of the peak near maximum is reproduced well by a Gaussian profile positioned at 17261.3 cm^{-1} with the width of 0.4 cm^{-1} FWHM, the latter being the instrumental width of two-color excitation (Fig.13b, dashed blue curve). In absorption experiments [48], the antihole was shifted in the absorption spectrum when the laser was fixed on another peak of the M center, but the sum of the laser and antihole position energies remained constant. The same behavior was observed here. The spectral maximum at 579.330 nm (ω = 17261.3 cm^{-1}) has the energy that, in combination with the dye laser, gives the energy of two exciton state

$2\omega_0$ = 34520.4 cm^{-1}. The corresponding position of ω_0 = 17260.2 cm^{-1} is shown in Fig. 3 by vertical dashed line.

In addition to sharp peak governed by $\omega_{dye} + \omega_{OPO} = 2\omega_0$ equation, there are two broad excitation bands from both sides of the peak (Fig. 13b, dark green line). Such bands were not observed in absorption experiments [48]. Here, they are the result of other excitation channels initiated by intense biharmonic excitation.

In general, four excitation channels leading to biexciton formation are possible under biharmonic pumping by fixed dye and tuned OPO (Fig. 14). Two types of the excitation pathways involve the combinations of dye+OPO and OPO+dye photons shown in Figs. 14a and 14b. Direct two-photon processes (Fig. 14a) proceed via one-exciton state sublevels without other intermediate processes, while the pathways in Fig. 14b involve phonon-induced population redistribution between one-exciton state sublevels [52].

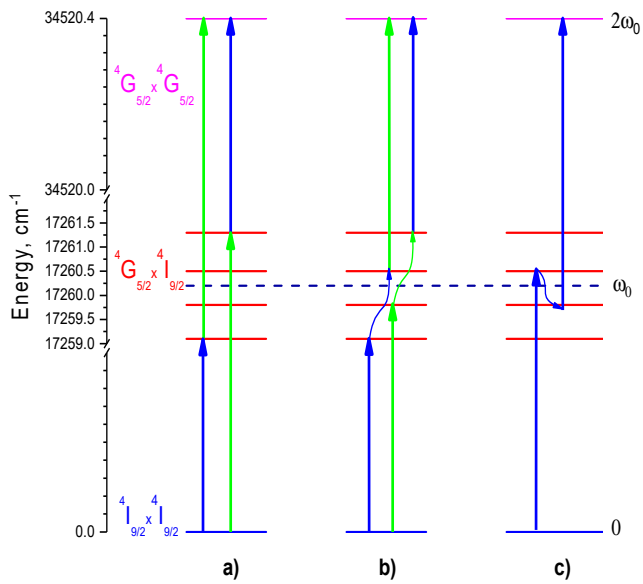

Fig. 14. Energy level diagram of M centers in Nd^{3+}: CaF_2 with the main channels of two-photon excitation for the formation of biexciton: (a) – direct two-color excitation by dye+OPO and OPO+dye; (b) – two-color excitation by dye+OPO and OPO+dye involving population redistribution between one-exciton state sublevels; (c) – single-color excitation by OPO+OPO involving population transfer between one-exciton state sublevels.

The other two of four excitation channels are single-color ones resulting from the combinations of two photons with equal energies as OPO+OPO and dye+dye. For the fixed dye laser, the latter channel can be neglected since it

adds only a constant background, if any, to the spectra. Therefore, only OPO+OPO will be considered as the actual one-color excitation pathway.

The process dye+OPO is just the process responsible for the formation of sharp peak considered above. For another two-color channel OPO+dye, the sum energy of two photon is the same, but another one-exciton sublevel is involved at the first step of two-photon absorption (Fig. 14a). Since OPO is scanned over all the spectral range of one-exciton state, it results in the formation of broad excitation band in the detected spectra. In particular, this channel is responsible for the formation of high-energy wing of the main peak.

The processes of two-photon excitation (Fig. 14a) are associated with the excitation of an intermediate one-exciton state. However, for any selected sublevel there is always the possibility of redistribution of the population over other nonresonant sublevels due to non-radiative processes associated with the absorption and emission of phonons [22, 45]. As a result of two-phonon Raman processes [52] all other sublevels become involved into the excitation of two-exciton state (Fig. 14b). Even though it is less effective channel than the direct two-photon excitation (Fig. 14a), it contributes to the detected upconversion excitation spectra.

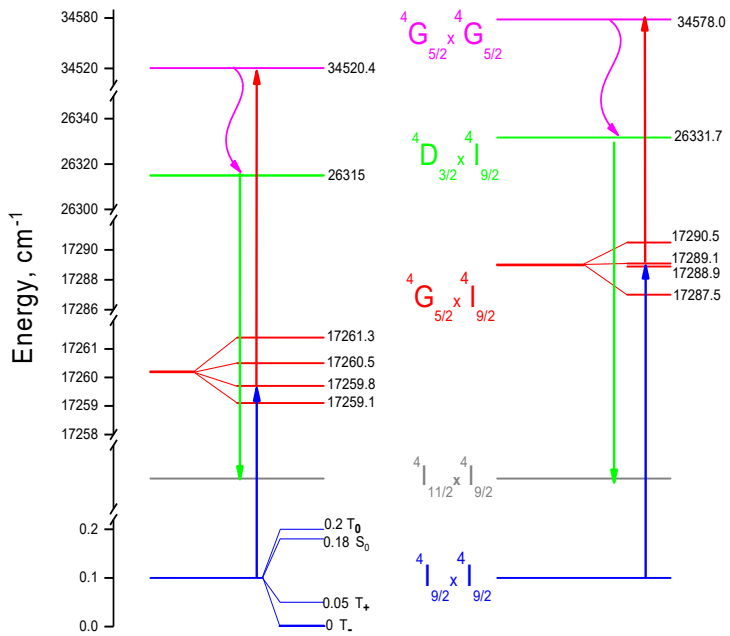

Fig. 15. Energy level diagram illustrating the excitation and detection of upconversion luminescence of the pair M center in the Nd^{3+}: CaF_2 (left) and M_1 center in the Nd^{3+}: SrF_2 (right) crystals. The one-exciton levels consist of four bright and four dark sublevels; the energies of two bright sublevels almost coincide; the energies of three dark sublevels also almost coincide with the energies of bright sublevels (for more details, see below the theoretical model of electronic states of the M center).

Furthermore, the processes involving intermediate population redistribution are responsible for the formation of specific excitation band near ω_0 registered under one-color excitation (Fig. 16, green curve). Such band, resulting from OPO+OPO process, is present in all the detected one- and two-color excitation spectra. In particular, the upconversion peak (Fig. 16, green curve) results from the excitation of the most intense peak in the one-exciton spectrum followed by relaxation to neighboring lower-lying level (Fig. 14c). Further absorption of another photon gives exactly the total excitation energy of $2\omega_0$ leading to the formation of the two-exciton state.

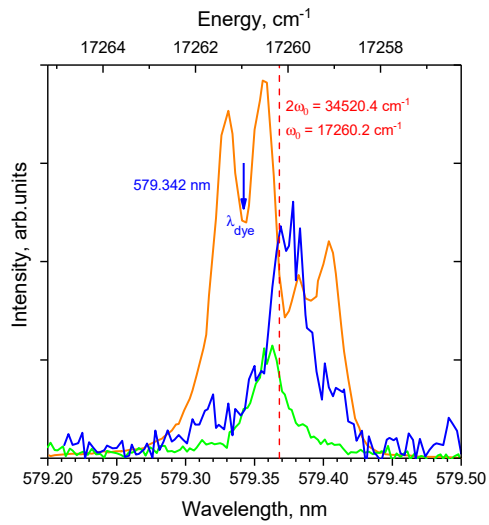

Fig. 16. Time-resolved fluorescence excitation spectra of 0.6% Nd^{3+}: CaF_2 crystal at T = 6.5K measured by scanning OPO at the $^4I_{9/2}(1) \rightarrow {}^4G_{5/2}(1)$ transition: NIR fluorescence recorded at the $^4F_{3/2}(1) \rightarrow {}^4I_{9/2}(1)$ transition at 863.56 nm – orange curve; upconversion UV fluorescence recorded at the $^4D_{3/2}(1) \rightarrow {}^4I_{11/2}(1)$ transition at 380.98 nm: under excitation by tuned OPO – green curve; under simultaneous excitation by tuned OPO and dye laser fixed at 579.344 nm (shown by arrow) – blue curve. The position of ω_0 is shown by vertical dashed line.

When the fixed position of the laser is detuned from any maximum of the one-exciton band towards nearby minimum, the intensity of the sharp peak rapidly decreases, since the number of corresponding M centers in the wings of the inhomogeneously broadened lines is greatly reduced. An example of UV excitation spectrum obtained with dye laser fixed in one of the minima of excitation band is shown in Fig. 16, blue curve. In this case, the excitation profile is obtained due to predominance of one- and two-color OPO+OPO and OPO+dye processes, while no sharp peak from the dye+OPO process is detected.

V. SUMMARY

The goal of the thesis was to study various fluoride crystals such as LaF_3, CaF_2, SrF_2 doped with Nd^{3+} ions using laser site-selective and kinetic spectroscopy, and to study the entangled quantum state of the pairs of Nd^{3+} ions. The following results were obtained:

1) Several previously undescribed optical centers of Nd^{3+} in LaF_3, CaF_2, SrF_2 crystals were discovered and described for the first time, including
   a) pair, triple, and quad optical centers of the Nd^{3+} ions in the 1% Nd^{3+}: LaF_3 crystal at T = 1.6K including the development of the method for determination of the number of ions in the cluster optical centers in the 1% Nd^{3+}: LaF_3 crystal at 1.6K via the measured lifetimes determined from the selective fluorescence decay kinetics of the metastable $^4F_{3/2}(1)$ crystal-field level;
   b) the nearly cubic sites of the Nd^{3+} ion with a symmetry close to O_h with a very long radiative lifetime of the $^4F_{3/2}(1)$ crystal-field level (τ_R = 13.6 ms) were found in an Nd^{3+}: Na^+: CaF_2 single crystal at T = 7 K using time-resolved site-selective laser spectroscopy; an optical site with a radiative lifetime of τ_R = 8.5 ms was found and assigned to have the C_{2v} symmetry, when the Na^+ ion replaces the Ca^{2+} ion in one of the positions adjacent to the Nd^{3+} ion in order to compensate the additional charge;
   c) two types of the pair centers denoted as M_1 and M_2 in the Nd^{3+}: SrF_2 crystal at T = 6.5 K, were found, spectrally shifted relative to each other by about 2 $см^{-1}$.
2) Time-resolved site-selective laser spectroscopy of the Nd^{3+}: CaF_2 crystal confirmed the splitting of the one-exciton $^4G_{5/2}(1)$ x $^4I_{9/2}(1)$ state of the pair M center of Nd^{3+} ions into four sublevels, at low temperatures with an energy difference ~1 cm^{-1}, and a significant inhomogeneous splitting of several cm^{-1} of the one-exciton state of the pair centers of the Nd^{3+} ions in the Nd^{3+}: SrF_2 crystal.
3) It was demonstrated for the first time that the Judd-Ofelt approach gives not only the rates of radiative relaxation of excited states of a rare-earth ion in different crystal matrices, but also a difference in the rates of emission of an excited state in different optical sites of the same ion in the same crystal matrix.
4) It was shown that the reason for the observed splitting of the one-exciton state in the Nd^{3+}: SrF_2 and Nd^{3+}: CaF_2 crystals is a strong resonance exchange of electronic excitation between two Nd^{3+} ions in a pair. Spin-orbit interaction allows this exchange of electronic excitation between Nd^{3+} ions in the M center to occur with spin flip.

SUMMARY IN ESTONIAN

Nd^{3+} ioonide optilised tsentrid ja kvantpõimitud seisundid dopeeritud fluoriid-kristallides

Doktoritöö eesmärgiks oli laserkohtselektiivse ja kineetilise spektroskoopia abil uurida erinevaid Nd^{3+} ioonidega dopeeritud fluoriidi kristalle (LaF_3, CaF_2, SrF_2) ning uurida Nd^{3+} ioonide paaride põimunud kvantseisundit. Saadi järgmised tulemused:

1) Esimest korda leiti ja kirjeldati mitmeid varem kirjeldamata Nd^{3+} optilisi tsentreid LaF_3, CaF_2, SrF_2 kristallides, sealhulgas:
   a) Nd^{3+} ioonide optilised paari-, kolmik- ja nelik-tsentrid 1% Nd^{3+}: LaF_3 kristallis T = 1,6 K juures, sealhulgas meetodi väljatöötamine ioonide arvu määramiseks klastri optilistes tsentrites 1% Nd^{3+}: LaF_3 kristallis temperatuuri 1,6 K juures mõõdetud eluea kaudu, mis on määratud metastabiilse $4F_{3/2}(1)$ kristallivälja seisundi selektiivse fluorestsentsi lagunemise kineetika põhjal;
   b) kasutades aeglahutusega kohtselektiivset laserspektroskoopiat leiti Nd^{3+}: Na^+: CaF_2 monokristallis temperatuuril T = 7 K Nd^{3+} iooni peaaegu kuubi sarnased saidid, mille sümmeetria on O_h-le lähedane ja mille kiirguse eluiga on väga pikk $^4F_{3/2}(1)$ kristallivälja seisundi korral (τR = 13.6 ms); leiti optiline koht kiirguse elueaga τR = 8.5 ms ja määrati selles C_{2v} sümmeetria, kui Na^+ ioon asendab Ca^{2+} iooni ühes Nd^{3+} iooniga külgnevatest positsioonidest, et kompenseerida lisalaengut;
   c) leiti kahte tüüpi paaritsentreid, mis on kristallis Nd^{3+}: SrF_2 temperatuuri T = 6,5 K juures tähistatud kui M_1 ja M_2 ja spektraalselt nihkunud üksteise suhtes umbes 2 cm^{-1} võrra.
2) Nd^{3+}: CaF_2 kristalli aeglahutusega kohtselektiivne laserspektroskoopia kinnitas Nd^{3+} ioonide paari M-tsentri $^4G_{5/2}(1)$ x $^4I_{9/2}(1)$ ühe-eksitonilise seisundi jagunemist neljaks alamnivooks madalatel temperatuuridel energia erinevusega ~1 cm^{-1}; ja Nd^{3+} ioonide paaritsentrite ühe-eksitonilise seisundi olulist mittehomogeenset jagunemist mitme cm^{-1} suurusjärgus Nd^{3+}: SrF_2 kristalli korral.
3) Esimest korda demonstreeriti, et Judd-Ofelti lähenemisviis ei anna mitte ainult haruldaste muldmetallide ioonide ergastatud olekute kiirgusrelaksatsiooni määrasid erinevates kristallimaatriksites, vaid ka erinevust ergastatud oleku emissiooni kiirustes sama iooni erinevates optilistes kohtades samas kristallmaatriksis.
4) Näidati, et Nd^{3+}: SrF_2 ja Nd^{3+}: CaF_2 kristallides täheldatud ühe-eksitonilise seisundi lõhenemise põhjuseks on elektroonse ergastuse tugev resonantsvahetus kahe Nd^{3+} iooni vahel paaris. Spin-orbiidi interaktsioon võimaldab seda elektroonilise ergastuse vahetust Nd^{3+} ioonide vahel M-tsentris spinnide pööramise korral.

REFERENCES

[1] J.W. Hodby, Electronic Properties, in: W. Hayes (Ed.) Crystals with the fluorite structure, Clarendon Press, London, 1974, pp. 1–42.

[2] D.C. Harris, Durable 3–5 μm transmitting infrared window materials, Infrared Physics & Technology, 39 (1998) 185–201.

[3] J.M. Baker, Rare-earth and other impurity ions in non-cubic sites, in: W. Hayes (Ed.) Crystals with the fluorite structure, Clarendon Press, London, 1974, pp. 341–414.

[4] C. Webb, J.D.C. Jones, Laser Design and Laser Systems, Boca Raton, 2003.

[5] A.A. Kaminskii, Laser Crystals: Their Physics and Properties, Springer Berlin, Heidelberg, 1990.

[6] H. Chen, A. Ikesue, H. Noto, H. Uehara, Y. Hishinuma, T. Muroga, R. Yasuhara, Nd^{3+}-activated CaF_2 ceramic lasers, Opt. Lett., 44 (2019) 3378–3381.

[7] B.M. Walsh, Judd-Ofelt theory: principles and practices, in: B. Di Bartolo, O. Forte (Eds.) Advances in Spectroscopy for Lasers and Sensing, Springer Netherlands, Dordrecht, 2006, pp. 403–433.

[8] B.R. Judd, Optical Absorption Intensities of Rare-Earth Ions, Physical Review, 127 (1962) 750–761.

[9] G.S. Ofelt, Intensities of Crystal Spectra of Rare-Earth Ions, The Journal of Chemical Physics, 37 (1962) 511–520.

[10] M. Mansmann, Die Kristall struktur von Lanthantrifluorid, 122 (1965) 375–398.

[11] V.V. Osiko, Y.K. Voron'ko, A.A. Sobol, Spectroscopic Investigations of Defect Structures and Structural Transformations in Ionic Crystals, in: H.C. Freyhardt, G. Müller (Eds.) Growth and Defect Structures, Springer Berlin Heidelberg, Berlin, Heidelberg, 1984, pp. 37–86.

[12] J. Corish, C.R.A. Catlow, P.W.M. Jacobs, S.H. Ong, Defect aggregation in anion-excess fluorites. Dopant monomers and dimers, Physical Review B, 25 (1982) 6425–6438.

[13] P.J. Bendall, C.R.A. Catlow, J. Corish, P.W.M. Jacobs, Defect aggregation in anion-excess fluorites II. Clusters containing more than two impurity atoms, Journal of Solid State Chemistry, 51 (1984) 159–169.

[14] T.P.J. Han, G.D. Jones, R.W.G. Syme, Site-selective spectroscopy of Nd^{3+} centers in CaF_2Nd^{3+} and SrF_2Nd^{3+}, Physical Review B, 47 (1993) 14706–14723.

[15] S.A. Payne, J.A. Caird, L.L. Chase, L.K. Smith, N.D. Nielsen, W.F. Krupke, Spectroscopy and gain measurements of Nd^{3+} in SrF_2 and other fluorite-structure hosts, J. Opt. Soc. Am. B, 8 (1991) 726–740.

[16] J. Nelson, Laser and infrared spectroscopy of Nd^{3+} and Pr^{3+} ions in fluorite crystals, in: Faculty of Science, University of Canterbury, University of Canterbury. Physics, 2003, pp. 170.

[17] B.C. Tofield, H.P. Weber, Efficient phonon-assisted long-lifetime $Nd^{3+}Cs_2NaNdCl_6$, Physical Review B, 10 (1974) 4560–4567.

[18] N.E. Kask, L.S. Kornienko, EPR of Nd3 Ions in Fluorite, Journal of Experimental and Theoretical Physics, 26 (1967) 331–335.

[19] Y.K. Voron'ko, K. A.A, V.V. Osiko, Analysis of the Optical Spectra of CaF_2:Nd^{3+} (Type 1) Crystals, Journal of Experimental and Theoretical Physics, 22 (1966) 295–300.

[20] N.E. Kask, L.S. Kornienko, M. Fakir, Electronic paramagnetic resonance and spinlattice relaxation of Nd^{3+} ions in monocrystals of CaF_2 (rus), Phys. Solid State, 6 (1964) 549–553.
[21] Y.V. Orlovskii, V.V. Fedorov, T.T. Basiev, M. Altwein, B. Leu, J. Heber, S. Mirov, Nonradiative relaxation and inhomogeneous splitting of aggregated optical centers in the Nd3+-doped CaF_2 and SrF_2 crystals (FLN and decay study), Journal of Luminescence, 83–84 (1999) 361–366.
[22] Y.V. Orlovskii, T.T. Basiev, A.G. Papashvili, I.N. Vorob'ev, O.K. Alimov, V.V. Osiko, J. Heber, Inhomogeneous broadening of the dynamically split Kramers spectral line and up-conversion in the pair and quartet centers in CaF_2:Nd^{3+}, Journal of Luminescence, 99 (2002) 223–236.
[23] T.T. Basiev, V. V., M.Y. Glotova, A.G. Papashvili, A.Y. Karasik, One- and two-photon spectra of Nd^{3+} clusters in CaF_2 and SrF_2 crystals, Quantum Electronics, 33 (2003) 684.
[24] Y. Orlovskii, T.T. Basiev, I.N. Vorob'Ev, V.V. Osiko, A.G. Papashvili, A.M. Prokhorov, Site-selective measurements of $^4G_{5/2}$; $^2G_{7/2}$ nonradiative relaxation rate in Nd : SrF_2, Nd : La : SrF_2, and Nd : Sr : LaF_3 laser crystals, Laser Physics, 6 (1996) 448–455.
[25] Y.V. Orlovskii, T.T. Basiev, V.V. Osiko, H. Gross, J. Heber, Fluorescence line narrowing (FLN) and site-selective fluorescence decay of Nd^{3+} centers in CaF_2, Journal of Luminescence, 82 (1999) 251–258.
[26] G. Vincow, W. Low, Paramagnetic Resonance Spectra of Nd^{3+} Ions in a Cubic Site, Physical Review, 122 (1961) 1390–1392.
[27] E. Vinogradova, L. Dolgov, V.A. Konyushkin, E.O. Orlovskaya, E.A. Vagapova, A. Treshchalov, V. Peet, V. Hizhnyakov, Y.V. Orlovskii, Fluorescence of Nd^{3+} optical centers close to cubic symmetry in a calcium fluoride crystal co-doped with Na^+, Journal of Luminescence, 234 (2021).
[28] V. Hizhnyakov, V. Boltrushko, H. Kaasik, Y. Orlovskii, Rare earth ions doped mixed crystals for fast quantum computers with optical frequency qubits, Optics Communications, 485 (2021) 126693.
[29] J. Wesenberg, K. Mølmer, Robust quantum gates and a bus architecture for quantum computing with rare-earth-ion-doped crystals, Physical Review A, 68 (2003) 012320.
[30] N. Ohlsson, R. Krishna Mohan, S. Kröll, Quantum computer hardware based on rare-earth-ion-doped inorganic crystals, Optics Communications, 201 (2002) 71–77.
[31] M. Nilsson, L. Rippe, N. Ohlsson, T. Christiansson, S. Kröll, Initial Experiments Concerning Quantum Information Processing in Rare-Earth-Ion Doped Crystals, Physica Scripta, 2002 (2002) 178.
[32] I. Roos, K. Mølmer, Quantum computing with an inhomogeneously broadened ensemble of ions: Suppression of errors from detuning variations by specially adapted pulses and coherent population trapping, Physical Review A, 69 (2004) 022321.
[33] E. Fraval, M.J. Sellars, J.J. Longdell, Dynamic Decoherence Control of a Solid-State Nuclear-Quadrupole Qubit, Physical Review Letters, 95 (2005) 030506.
[34] L. Rippe, M. Nilsson, S. Kröll, R. Klieber, D. Suter, Experimental demonstration of efficient and selective population transfer and qubit distillation in a rare-earth-metal-ion-doped crystal, Physical Review A, 71 (2005) 062328.

[35] J.H. Wesenberg, Designing robust gate implementations for quantum-information processing, Physical Review A, 69 (2004) 042323.
[36] J.H. Wesenberg, K. Mølmer, L. Rippe, S. Kröll, Scalable designs for quantum computing with rare-earth-ion-doped crystals, Physical Review A, 75 (2007) 012304.
[37] E. Saglamyurek, N. Sinclair, J. Jin, J.A. Slater, D. Oblak, F. Bussières, M. George, R. Ricken, W. Sohler, W. Tittel, Conditional Detection of Pure Quantum States of Light after Storage in a Tm-Doped Waveguide, Physical Review Letters, 108 (2012) 083602.
[38] Y. Yan, J. Karlsson, L. Rippe, A. Walther, D. Serrano, D. Lindgren, M.-e. Pistol, S. Kröll, P. Goldner, L. Zheng, J. Xu, Measurement of linewidths and permanent electric dipole moment change of the Ce ^{4}f - ^{5}d transition in Y_2SiO_5 for qubit readout scheme in rare-earth ion based quantum computing, Physical Review B, 87 (2013) 184205.
[39] D. Serrano, J. Karlsson, L. Zheng, Y. Dong, A. Ferrier, P. Goldner, A. Walther, L. Rippe, S. Kröll, Satellite line mapping in Eu^{3+}–Ce^{3+} and Pr^{3+}–Ce^{3+} codoped Y_2SiO_5, Journal of Luminescence, 170 (2016) 102–107.
[40] L. Rippe, B. Julsgaard, A. Walther, Y. Ying, S. Kröll, Experimental quantum-state tomography of a solid-state qubit, Physical Review A, 77 (2008) 022307.
[41] A. Walther, B. Julsgaard, L. Rippe, Y. Ying, S. Kröll, R. Fisher, S. Glaser, Extracting high fidelity quantum computer hardware from random systems, Physica Scripta, 2009 (2009) 014009.
[42] A. Walther, L. Rippe, Y. Yan, J. Karlsson, D. Serrano, A.N. Nilsson, S. Bengtsson, S. Kröll, High-fidelity readout scheme for rare-earth solid-state quantum computing, Physical Review A, 92 (2015) 022319.
[43] J.G. Bartholomew, T. Zhong, J.M. Kindem, R. Lopez-Rios, J. Rochman, I. Craiciu, E. Miyazono, A. Faraon, Controlling rare-earth ions in a nanophotonic resonator using the ac Stark shift, Physical Review A, 97 (2018) 063854.
[44] T.T. Basiev, A.Y. Karasik, V.V. Fedorov, K.W. Ver Steeg, Optical echo spectroscopy and phase relaxation of Nd^{3+} ions in CaF_2 crystals, Journal of Experimental and Theoretical Physics, 86 (1998) 156–163.
[45] T.T. Basiev, V.V. Fedorov, A.Y. Karasik, K.K. Pukhov, Strong coherent interaction of Nd^{3+}–Nd^{3+} pair ions in CaF_2 crystal, Journal of Luminescence, 81 (1999) 189–197.
[46] S.K. Sekatskii, T.T. Basiev, I.T. Basieva, G. Dietler, V.V. Fedorov, A.Y. Karasik, Y.V. Orlovskii, K.K. Pukhov, Experimental preparation of entangled Bell's vacuum–single exciton and vacuum–biexciton states for pair centers of neodymium ions in a crystal, Optics Communications, 259 (2006) 298–303.
[47] Y.V. Orlovskii, E.A. Vagapova, V. Peet, E. Vinogradova, L. Dolgov, V. Boltrushko, V. Hizhnyakov, One- and two-exciton states of pair centers of Kramers Nd^{3+} ions in Nd-doped CaF_2 and SrF_2 crystals, and their possible use as qubits, Journal of Luminescence, 251 (2022) 119218.
[48] V.V. Fedorov, W. Beck, T.T. Basiev, A.Y. Karasik, C. Flytzanis, Fine level splitting of aggregate neodymium centers in CaF_2 crystals, Chemical Physics, 257 (2000) 275–281.
[49] Y.V. Orlovskii, A.V. Popov, E.O. Orlovskaya, A.S. Vanetsev, E.A. Vagapova, M. Rähn, V. Sammelselg, I. Sildos, A.E. Baranchikov, P.V. Grachev, V.B. Loschenov, A.V. Ryabova, Comparison of concentration dependence of relative fluorescence quantum yield and brightness in first biological window of wavelengths for

aqueous colloidal solutions of Nd^{3+}: LaF_3 and Nd^{3+}: KY_3F_{10} nanocrystals synthesized by microwave-hydrothermal treatment, Journal of Alloys and Compounds, 756 (2018) 182–192.
[50] Y.V. Orlovskii, H. Gross, E.E. Vinogradova, V. Boltrushko, V. Hizhnyakov, Spectroscopic evidence of cooperative (entangled) quantum states of Nd^{3+} ion pairs in Nd^{3+}: LaF_3 crystal, Journal of Luminescence, 219 (2020) 116920.
[51] A.M. Stoneham, Shapes of Inhomogeneously Broadened Resonance Lines in Solids, Rev. Mod. Phys., 41 (1969) 82–108.
[52] D.L. Huber, M.M. Broer, B. Golding, Low-Temperature Optical Dephasing of Rare-Earth Ions in Glass, Physical Review Letters, 52 (1984) 2281–2284.

ACKNOWLEDGEMENTS

I am very grateful to my supervisors Yu.V. Orlovskiy, V. Peet, and I. Sildos for support and guidance. Also, I am thankful to all colleges from the Laboratory of Laser Spectroscopy, Institute of Physics and especially L. Dolgov, L. Puust, for their assistant with experimental work, V. Hižnjakov, for his assistance with theoretical work, V.A. Konyushkin and E.O. Orlovskaya for synthesis of the samples, and E.A. Vagapova for her assistance with experimental work and overall support.

I acknowledge the Estonian Research Council (grant PRG347) for financial support.

PUBLICATIONS

CURRICULUM VITAE

Name	Elena Vinogradova
Date of birth	January 15, 1991
Phone	+372 5891 0780
ORCID	0000-0002-8222-8927
E-mail	elena.vinogradova@ut.ee

Education:

2018	M.Sc. Moscow Power Engineering Institute, Quantum Electronics, Moscow, Russia
2016	2015 B.Sc. Moscow Power Engineering Institute, Quantum Electronics, Moscow, Russia

Publications included in the thesis:

1. Orlovskii, Yu.V.; Vagapova, E.A.; Peet, V.; Vinogradova, E.; Dolgov, L.; Boltrushko, V.; Hizhnyakov, V. (2022). One- and two-exciton states of pair centers of Kramers Nd^{3+} ions in Nd-doped CaF_2 and SrF_2 crystals, and their possible use as qubits. Journal of Luminescence, 251, 119218. DOI: 10.1016/j.jlumin.2022.119218.
2. Vinogradova, E.; Dolgov, L.; Konyushkin, V.A.; Orlovskaya, E.O.; Vagapova, E.; Treshchalov, A.; Peet, V.; Hizhnyakov, V.; Orlovskii; Yu.V. (2021). Fluorescence of Nd^{3+} optical centers close to cubic symmetry in a calcium fluoride crystal co-doped with Na^{+}. Journal of Luminescence, 234, 117988. DOI: 10.1016/j.jlumin.2021.117988.
3. Orlovskii, Yu V.; Gross, H.; Vinogradova, E.E.; Boltrushko, V.; Hizhnyakov, V. (2020). Spectroscopic evidence of cooperative (entangled) quantum states of Nd^{3+} ion pairs in Nd^{3+}: LaF_3 crystal. Journal of Luminescence, 116920. DOI: 10.1016/j.jlumin.2019.116920.

International conferences presentations related to the thesis:

1. Orlovskii Yu., Vagapova E., Peet V., Vinogradova E, Dolgov L., Boltrushko V., Hizhnyakov V. (2022). Entangled States in Nd^{3+} Doped Crystals With Fluorite Structure as Qubits. *48th European Conference on Optical Communication, Basel, Switzerland, 18−22 September 2022.* Optica Publishing Group.
2. Orlovskii, Y.; Vinogradova, E.; Hiznyakov, V. (2019). Cooperative States of Nd^{3+} Ion Pairs and Clusters in Nd^{3+}: LaF_3 crystal. *Conference on Lasers and Electro-Optics Europe & European Quantum Electronics Conference, Munich, Germany, 23 – 27 June.* IEEE, eb-p-13.
3. Vinogradova, E.; Vagapova, E.; Dolgov, L.; Orlovskii, Yu. (2019). Rare earth ions optical centers in inorganic phosphors: from single to entangled states prospective for quantum computing. *Abstract book International research and practice conference Nanotechnology and nanomaterials*

NANO-2019. LLC Computer-publishing information center, Kiev, Ukraine, 668−668.

Other publications:

1. Miller, Caius; Puust, Laurits; Ekimov, Evgeny; Vlasov, Igor; Vanetsev, Alexander; Vinogradova, Elena; Orlovskii, Yurii; Treshchalov, Aleksei; Sildos, Ilmo (2021). Toward Performance and Applications of Large Area Optical Thermometry Based on the Luminescence of Germanium-Vacancy Defects in Diamond Nanocrystals. Physica status solidi (a), 2000217. DOI: 10.1002/pssa.202000217.

ELULOOKIRJELDUS

Nimi: Elena Vinogradova
Sünniaeg 15. jaanuar 1991
Telefon +372 5891 0780
ORCID 0000-0002-8222-8927
E-post elena.vinogradova@ut.ee

Haridustee:

2018 M.Sc. Moskva energeetikainstituut, kvant- ja optiline elektroonika, Moskva, Venemaa

2016 B.Sc. Moskva energeetikainstituut, kvant- ja optiline elektroonika, Moskva, Venemaa

Teeside aluseks olevate publikatsioonide loetetu:

1. Orlovskii, Yu.V.; Vagapova, E.A.; Peet, V.; Vinogradova, E.; Dolgov, L.; Boltrushko, V.; Hizhnyakov, V. (2022). One- and two-exciton states of pair centers of Kramers Nd^{3+} ions in Nd-doped CaF_2 and SrF_2 crystals, and their possible use as qubits. Journal of Luminescence, 251, 119218. DOI: 10.1016/j.jlumin.2022.119218.
2. Vinogradova, E.; Dolgov, L.; Konyushkin, V.A.; Orlovskaya, E.O.; Vagapova, E.; Treshchalov, A.; Peet, V.; Hizhnyakov, V.; Orlovskii; Yu.V. (2021). Fluorescence of Nd^{3+} optical centers close to cubic symmetry in a calcium fluoride crystal co-doped with Na^{+}. Journal of Luminescence, 234, 117988. DOI: 10.1016/j.jlumin.2021.117988.
3. Orlovskii, Yu V.; Gross, H.; Vinogradova, E.E.; Boltrushko, V.; Hizhnyakov, V. (2020). Spectroscopic evidence of cooperative (entangled) quantum states of Nd^{3+} ion pairs in Nd^{3+}: LaF_3 crystal. Journal of Luminescence, 116920. DOI: 10.1016/j.jlumin.2019.116920.

Osalemine rahvusvahelistel teaduskonverentsidel::

1. Orlovskii Yu., Vagapova E., Peet V., Vinogradova E, Dolgov L., Boltrushko V., Hizhnyakov V. (2022). Entangled States in Nd^{3+} Doped Crystals With Fluorite Structure as Qubits. *48th European Conference on Optical Communication, Basel, Switzerland, 18−22 September 2022.* Optica Publishing Group.
2. Orlovskii, Y.; Vinogradova, E.; Hiznyakov, V. (2019). Cooperative States of Nd^{3+} Ion Pairs and Clusters in Nd^{3+}: LaF_3 crystal. *Conference on Lasers and Electro-Optics Europe & European Quantum Electronics Conference, Munich, Germany, 23–27 June.* IEEE, eb-p-13.
3. Vinogradova, E.; Vagapova, E.; Dolgov, L.; Orlovskii, Yu. (2019). Rare earth ions optical centers in inorganic phosphors: from single to entangled states prospective for quantum computing. *Abstract book International research and practice conference Nanotechnology and nanomaterials*

NANO-2019. LLC Computer-publishing information center, Kiev, Ukraine, 668−668.

Autori muud publikatsioonid:

1. Miller, Caius; Puust, Laurits; Ekimov, Evgeny; Vlasov, Igor; Vanetsev, Alexander; Vinogradova, Elena; Orlovskii, Yurii; Treshchalov, Aleksei; Sildos, Ilmo (2021). Toward Performance and Applications of Large Area Optical Thermometry Based on the Luminescence of Germanium-Vacancy Defects in Diamond Nanocrystals. physica status solidi (a), 2000217. DOI: 10.1002/pssa.202000217.

DISSERTATIONES SCIENTIAE MATERIALIS UNIVERSITATIS TARTUENSIS

1. **Martin Järvekülg**. Tubular microstructures by Hf-, Zr- and Ti-butoxide gel sheet rolling. Tartu, 2011, 112 p.
2. **Sergei Vlassov.** Investigation of nanoscale interactions and mechanical properties of nanostructures using quartz tuning fork based real-time measurements. Tartu, 2011, 171 p.
3. **Margus Kodu**. Pulsed Laser Deposition of Magnesium Oxide and Barium Ternary Oxides for Plasma Display Protective Layers. Tartu, 2011, 89 p.
4. **Rainer Pärna**. Surface studies of some oxide films. Tartu, 2011, 129 p.
5. **Jevgeni Šulga**. Self-assembly and interaction of nanostructures. Tartu, 2011, 114 p.
6. **Wojciech Kuznik**. Quantum-chemical computer simulations of the linear and non-linear optical properties of pyrazoloquinoline and dicyanopyrazine derivatives. Tartu, 2012, 89 p.
7. **Leonid Dorogin**. Structural and tribological properties of zero- and one-dimensional nanocrystals. Tartu, 2012, 193 p.
8. **Viljar Palmre**. Fabrication and characterization of microporous carbon-based electroactive polymer actuators. Tartu, 2012, 99 p.
9. **Madis Paalo**. Synthesis of CNT-metal oxide nanocomposites: sol-gel process, rheology, structural and functional properties. Tartu, 2014, 175 p.
10. **Raul Välbe**. Developement of ionic liquid composites by sol-gel method for elaboration of industrial nano- and microstructures. Tartu, 2014, 97 p.
11. **Urmas Joost**. Impurity and preparation dependent properties of titania thin films. Tartu, 2014, 155 p.
12. **Madis Umalas**. Application of sol-gel technology for production of ceramic nanocomposites and functional coatings. Tartu, 2015, 136 p.
13. **Elena Samsonova**. Energy transfer probe as a tool to study morphological and structural origins of fluorescence quenching in rare-earth doped nanophosphors. Tartu, 2015, 114 p.
14. **Jay Mondal**. Novel Corrosion Protective Nanostructured Composite Coatings. Tartu, 2016, 104 p.
15. **Kathriin Utt**. Metal oxide mesostructures for optical applications. Tartu, 2016, 88 p.
16. **Kaido Siimon**. Electrospun gelatin cross-linked by glucose. Tartu, 2016, 84 p.
17. **Marko Part**. Combined three-dimensional sol-gel structures and atomic layer deposited thin films. Tartu, 2017, 162 p.
18. **Pejman Rasti**. Analysis of Remote Sensing Image Super Resolution using Fluid Lenses. Tartu, 2017, 188 p.
19. **Ivo Romet**. Recombination luminescence of doped borates: origin and application prospects in dosimetry. Tartu, 2017, 111 p.

20. **Vladimir I. Kondratiev**. Processing and characterization of transparent electrode materials. Tartu, 2017, 111 p.
21. **Taivo Jõgiaas**. Mechanical properties of atomic layer deposited thin films and nanocomposites. Tartu, 2017, 125 p.
22. **Lauri Aarik**. Atomic layer deposition and characterization of thin oxide films for application in protective coatings. Tartu, 2017, 180 p.
23. **Triin Kangur**. Preparation and functional properties of stochastic micro-structured sol-gel silica materials. Tartu, 2018, 96 p.
24. **Marta Berholts**. Fragmentation of ionic and hydrogen-bonded molecules induced by synchrotron radiation. Tartu, 2018, 126 p.
25. **Priit Priimägi**. Development and optimization of 3D-microbatteries. Tartu, 2018, 118 p.
26. **Siim Hödemann**. Residual stress determination in chemically strengthened and thermally tempered glass plates using scattered light method. Tartu, 2019, 146 p.
27. **Jekaterina Kozlova**. Complex characterization of graphene structures on nanometer level. Tartu, 2019, 206 p.
28. **Kristjan Kalam**. Magnetic, electric and structural properties of atomic layer deposited zirconia-based nanolaminates and mixtures. Tartu, 2020, 94 p.
29. **Triinu Vihmann**. Ionic liquids: synthesis and application in lubrication and lithography. Tartu, 2020, 102 p.
30. **Helina Seemen**. Atomic layer deposition and microscopic analysis of magnetically and electrically polarizable thin solid films. Tartu, 2021, 126 p.
31. **Ekaterina Vagapova.** Fluorescence quenching in inorganic crystalline solids activated by neodymium ions; from bulk to micro- and nanocrystals. Tartu, 2021, 116 p.
32. **Evgenii Strugovshchikov**. First-principles studies on rare-earth metal-hydride-based smart materials. Tartu, 2021, 166 p.
33. **Maido Merisalu**. Nanostructured Coatings for Car and Aerospace Industries. Tartu, 2022, 179 p.